Kinetic Mechanism of Nucleotide Cofactor Binding to *Escherichia coli* Replicative Helicase DnaB Protein. Stopped-Flow Kinetic Studies Using Fluorescent, Ribose-, and Base-Modified Nucleotide Analogues†

Wlodzimierz Bujalowski* and Maria J. Jezewska

Department of Human Biological Chemistry and Genetics, The University of Texas Medical Branch at Galveston, 301 University Boulevard, Galveston, Texas 77555-1053

Received October 18, 1999; Revised Manuscript Received December 6, 1999

ABSTRACT: The kinetic mechanism of binding nucleotide cofactors to the *Escherichia coli* primary replicative helicase DnaB protein has been studied, using the fluorescence stopped-flow technique. The experiments have been performed with fluorescent ATP and ADP analogues bearing the modification on the ribose, MANT-AMP-PNP and MANT-ADP, and on the base, ϵAMP-PNP and ϵADP. Association of the DnaB helicase with nucleotide cofactors is characterized by four relaxation times that indicate that the binding occurs by a minimum of four-steps. The simplest mechanism which can describe the data is a four-step sequential process where the bimolecular binding step is followed by three isomerization steps. This mechanism is described by the following equation: Helicase + N $\underset{k_{-1}}{\overset{k_1}{\rightleftharpoons}}$ $(H-N)_1$ $\underset{k_{-2}}{\overset{k_2}{\rightleftharpoons}}$ $(H-N)_2$ $\underset{k_{-3}}{\overset{k_3}{\rightleftharpoons}}$ $(H-N)_3$ $\underset{k_{-4}}{\overset{k_4}{\rightleftharpoons}}$ $(H-N)_4$. The binding mechanism is independent of the location of the nucleotide cofactor modification and is an intrinsic property of the DnaB helicase−nucleotide system. Quantitative amplitude analyses, using the matrix projection operator technique, allowed us to determine specific fluorescence changes accompanying the formation of all intermediates relative to the fluorescence of the free nucleotide. It shows that the major conformational change of the DnaB helicase−nucleotide complex occurs in the formation of the $(H-N)_1$. Moreover, the value of the bimolecular rate constant, k_1, is 3−4 orders of magnitude lower than the value expected for the diffusion-controlled reaction. These results indicate that the determined first step includes formation of the collision and an additional transition of the enzyme−nucleotide complex. The obtained results provide evidence of profoundly different conformational states of the ribose and base regions of the nucleotide-binding site in different intermediates. The sequential nature of the mechanism of the nucleotide binding to the DnaB helicase indicates the lack of the existence of a kinetically significant conformational equilibrium of the helicase protomer and the DnaB hexamer prior to the binding. The significance of these results for the functioning of the DnaB helicase is discussed.

The DnaB protein is an essential replication protein in *Escherichia coli*, which is involved in both the initiation and elongation stages of chromosomal DNA replication, as well as in the replication of phage and plasmid DNA (*1*, *2*). The protein is the *E. coli* primary replicative helicase, i.e., the factor responsible for unwinding the duplex DNA in front of the replication fork (*1*, *3*, *4*). The DnaB protein is the only helicase required to reconstitute DNA replication in vitro from the chromosomal origin of replication (oriC).

In solution, the DnaB helicase exists as a hexamer (*5*−*7*). Sedimentation equilibrium and sedimentation velocity studies show that the DnaB helicase forms a stable hexamer in a large protein concentration range, specifically stabilized by multiple magnesium cations (*6*, *7*). Hydrodynamic and E. M. data indicate that six protomers aggregate with cyclic symmetry in which the protomer−protomer contacts are limited to only two neighboring subunits (*6*, *8*, *9*). Thermodynamic studies provide direct evidence of the presence of long-range allosteric interactions in the hexamer encompassing all six subunits of the enzyme (*10*, *11*).

In the stationary complex with the ssDNA, i.e., without ATP hydrolysis, the DnaB helicase binds the nucleic acid with a stoichiometry of 20 ± 3 nucleotides/DnaB hexamer (*10*−*16*). Photo-cross-linking experiments indicate that in the stationary complex the ssDNA binds predominately to a single subunit of the hexamer (*10*, *12*). Thus, the DnaB hexamer has an effective, single binding site for the ssDNA; although, each subunit can most probably be initially selected for ssDNA binding. Fluorescence energy transfer studies show that the helicase binds the ssDNA in a single orientation

† This work was supported by NIH Grants GM-46679 and GM-58675 (to W.B.).

* To whom correspondence should be addressed. Phone: (409) 772-5634. Fax: (409) 772-1790. E-mail: wbujalow@utmb.edu.

10.1021/bi992413m CCC: $19.00
Published on Web 02/04/2000

with respect to the polarity of the sugar−phosphate backbone of the nucleic acid. Moreover, the same studies indicate that in the complex with the helicase the ssDNA passes through the cross-channel of the hexamer (*16*). Our thermodynamic studies also show that the total ssDNA binding site of the enzyme is built of two subsites, a strong and a weak ssDNA binding subsite, each of which encompasses ~10 nucleotide residues (*14*−*16*).

Helicases are motor proteins which utilize the energy from the nucleotide triphosphate hydrolysis to perform their functions, particularly unwinding of the duplex DNA and the mechanical translocation along the nucleic acid lattice (*17*). The activities of the DnaB protein in vivo are related to its ability to interact with both a ssDNA and a dsDNA that is under ATP control (*1*−*3*, *18*). Quantitative studies of nucleotide binding to the DnaB helicase have established that the hexamer has six nucleotide-binding sites, presumably one on each protomer (*18*, *19*−*22*). On the basis of thermodynamically rigorous fluorescence titrations, we determined that the binding process is biphasic. First, three nucleotide molecules bind independently in the high-affinity step and the next three nucleotides bind in the low-affinity step. The biphasic behavior of binding isotherms results from the negative cooperative interactions among binding sites (*19*−*22*).

Elucidation of nucleotide interactions with the DnaB protein is indispensable for understanding the different activities of the enzyme. This knowledge is a prerequisite for formulating any model of the mechanism of enzyme functioning in DNA replication, including translocation on the nucleic acid lattice and the catalysis of duplex DNA unwinding.

In this communication, as a first step on the way to understanding the dynamics of nucleotide cofactor binding to the DnaB helicase, we address the kinetics of nucleotide binding to the single, noninteracting site of the DnaB, using the fluorescent nucleotide analogues, β,γ-imido-1,N^6-ethenoadenosine-5′-triphosphate (ϵAMP-PNP),[1] 1,N^6-ethenoadenosine diphosphate (ϵADP), 3′(2′)-*O*-(*N*-methylantraniloyl) β,γ-imido-adenosine-5′-diphosphate (MANT-AMP-PNP), 3′(2′)-*O*-(*N*-methylantraniloyl) adenosine-5′-diphosphate (MANT-ADP) (*23*, *24*). These analogues differ by the type and location of the modifying groups. In the case of MANT-derivatives, the modification is located on the ribose, while the etheno-derivative is modified on the adenine residue (*19*−*24*). Our data show that the association of the nucleotide cofactor with the binding site on the DnaB hexamer proceeds through a complex, minimum four-step sequential mechanism. Amplitude analyses indicate that the major conformational transition of the enzyme−nucleotide complex occurs in the first step. The sequential character of the mechanism indicates that the association of a nucleotide with the single, noninteracting site of the DnaB hexamer is not preceded by a conformational transition of the protomer nor by the helicase hexamer prior to binding.

[1] Abbreviations: AMP-PNP, β,γ-imidoadenosine-5′-triphosphate; ϵAMP-PNP, β,γ-imido-1,N^6-ethenoadenosine-5′-triphosphate; ϵADP, 1,N^6-ethenoadenosine diphosphate; MANT-AMP-PNP, 3′(2′)-*O*-(*N*-methylantraniloyl) β,γ-imido-adenosine-5′-diphosphate; MANT-ADP, 3′(2′)-*O*-(*N*-methylantraniloyl) adenosine-5′-diphosphate, E. M., electron microscopy; Tris, tris(hydroxymethyl)aminomethane.

MATERIALS AND METHODS

Reagents and Buffers. All solutions were made with distilled and deionized >18 MΩ (Milli-Q Plus) water. All chemicals were of reagent grade. Buffer T2 is 50 mM Tris adjusted to pH 8.1 with HCl, 5 mM $MgCl_2$, and 10% glycerol. The temperature and concentration of NaCl in the buffer are indicated in the text.

DnaB Protein. The *E. coli* DnaB protein was purified, as previously described by us (*6*, *19*−*21*). The concentration of the protein was spectrophotometrically determined, using the extinction coefficient $\epsilon_{280} = 1.85 \times 10^5$ M^{-1} cm^{-1} (Hexamer) (*6*).

Nucleotides. MANT-AMP-PNP and MANT-ADP were synthesized as described by Hiratsuka (*24*). ϵAMP-PNP was synthesized using the method of Secrist et al. (*23*). ϵADP was from Sigma and used without further purification. All nucleotides used in the binding and kinetic studies were >95% pure as judged by TLC on silica. The concentrations of the nucleotides were determined using extinction coefficients $\epsilon_{356} = 5800$ M^{-1} cm^{-1} and $\epsilon_{294} = 2900$ M^{-1} cm^{-1} for MANT- and etheno-derivatives, respectively (*23*, *24*).

Stopped-Flow Kinetics. All fluorescence stopped-flow kinetic experiments were performed using either a SX.18MV stopped-flow or a SX.18MV sequential stopped-flow instrument (Applied Photophysics Ltd. Leatherhead, U.K.). The reactions were monitored using nucleotide cofactor fluorescence, with $\lambda_{ex} = 295$ and 325 nm for MANT-derivatives and etheno-derivatives, respectively. The emission was observed through a GG400 cutoff filter (Schott, PA) with the excitation monochromator slits at 1 mm (band-pass ≈ 4.5 nm). The experiments were performed in the "oversampling" mode in which the instrument collects and averages multiple data points at the fastest instrumental rate for the selected time interval, achieving a higher signal-to-noise ratio. Usually, three to eight traces were collected and averaged for each sample. The kinetic curves were fitted to extract relaxation times and amplitudes using nonlinear least-squares software provided by the manufacturer with the exponential function defined as

$$F(t) = F(\infty) + \sum_{i=1}^{n} A_i \exp(-\lambda_i t) \qquad (1)$$

where $F(t)$ is the fluorescence intensity at time t, $F(\infty)$ is the fluorescence intensity at $t = \infty$, A_i is the amplitude corresponding to ith relaxation process, λ_i is the time constant (reciprocal relaxation time) characterizing ith relaxation process, and n is the number of relaxation processes. All further analyses of the data were performed on MacIntosh G3 computers using Mathematica (Wolfram, Urbana, IL) and Kaleida Graph (Synergy Software, PA).

THEORY

Analysis of Stopped-Flow Kinetic Experiments Using the Matrix Projection Operator Technique. Quantitative determination of the mechanism of the macromolecule−ligand interactions, using spectroscopic stopped-flow measurements, requires the examination of both the relaxation times and

the amplitudes of the observed processes. In our analyses of the dynamics of the interactions of the DnaB helicase with nucleotides, we used the matrix projection operator technique (*25*). This powerful method is particularly useful for the analysis of spectroscopic stopped-flow kinetics, by providing closed-form explicit expressions for the amplitudes of the studied reactions. In turn, this allows the experimenter to obtain invaluable information on the structural and mechanical aspects of all identified intermediates unavailable by other methods.

As we show below, the dynamics of nucleotide cofactor binding to the DnaB helicase includes the bimolecular step that is followed by three first-order conformational transitions. This is a sequential reaction between nucleotide, N, and helicase, H, described by the equation

$$\mathrm{H} + \mathrm{N}_1 \underset{k_{-1}}{\overset{k_1}{\rightleftharpoons}} \mathrm{N}_2 \underset{k_{-2}}{\overset{k_2}{\rightleftharpoons}} \mathrm{N}_3 \underset{k_{-3}}{\overset{k_3}{\rightleftharpoons}} \mathrm{N}_4 \underset{k_{-4}}{\overset{k_4}{\rightleftharpoons}} \mathrm{N}_5 \qquad (2)$$

The reaction is monitored by the fluorescence change of the nucleotide. There are four relaxation times and four amplitudes, i.e., there are four normal modes of the reaction (*26*). The differential equations describing the time course of reaction 2, in terms of different nucleotide species, are

$$\frac{dN_1}{dt} = -k_1 H N_1 + k_{-1} N_2 \qquad (3a)$$

$$\frac{dN_2}{dt} = k_1 N_1 H - (k_{-1} + k_2) N_2 + k_{-2} N_3 \qquad (3b)$$

$$\frac{dN_3}{dt} k_2 N_2 - (k_{-2} + k_3) N_3 + k_{-3} N_4 \qquad (3c)$$

$$\frac{dN_4}{dt} = k_3 N_3 - (k_{-3} + k_4) N_4 + k_{-4} N_5 \qquad (3d)$$

$$\frac{dN_5}{dt} = k_4 N_4 - k_{-4} N_5 \qquad (3e)$$

Studies described in this work are performed in the large excess of the helicase over the nucleotide, $H_{tot} \gg N_{tot}$, i.e., H_{tot} is constant during the reaction. In matrix notation, system 3 is defined as

$$\begin{pmatrix} \frac{dN_1}{dt} \\ \frac{dN_2}{dt} \\ \frac{dN_3}{dt} \\ \frac{dN_4}{dt} \\ \frac{dN_5}{dt} \end{pmatrix} = \begin{pmatrix} -k_1 H & k_{-1} & 0 & 0 & 0 \\ k_1 H & -(k_{-1} + k_2) & k_{-2} & 0 & 0 \\ 0 & k_2 & -(k_{-2} + k_3) & k_3 & 0 \\ 0 & 0 & k_3 & -(k_3 + k_4) & k_{-4} \\ 0 & 0 & 0 & k_4 & -k_{-4} \end{pmatrix} \begin{pmatrix} N_1 \\ N_2 \\ N_3 \\ N_4 \\ N_5 \end{pmatrix} \qquad (4)$$

and

$$\dot{\mathbf{N}} = \mathbf{M}\mathbf{N} \qquad (5)$$

where $\dot{\mathbf{N}}$ is a vector of time derivatives, **M** is the coefficient matrix, and **N** is the vector of concentrations of different nucleotide forms in solution. In the standard matrix approach, the solution of system 4 is

$$\mathbf{N} = \exp(\mathbf{M}t)\mathbf{N_0} \qquad (6)$$

where

$$\exp(\mathbf{M}t) = \mathbf{V} \begin{pmatrix} \exp(\lambda_0 t) & 0 & 0 & 0 & 0 \\ 0 & \exp(\lambda_1 t) & 0 & 0 & 0 \\ 0 & 0 & \exp(\lambda_2 t) & 0 & 0 \\ 0 & 0 & 0 & \exp(\lambda_3 t) & 0 \\ 0 & 0 & 0 & 0 & \exp(\lambda_4 t) \end{pmatrix} \mathbf{V}^{-1} \qquad (7)$$

Quantities λ_0, λ_1, λ_2, λ_3, and λ_4 are eigenvalues of matrix **M**, **V** is a matrix whose columns are the eigenvectors of matrix **M**, and $\mathbf{N}_o$ is the vector of the initial concentrations. In the considered case of the sequential reaction, defined by eq 2, $\mathbf{N}_o$ is a column vector, (N_{tot}, 0, 0, 0, 0), where N_{tot} is the total concentration of the nucleotide. The elements of the vector $\mathbf{N}_o$ result from the fact that at $t = 0$, the concentration of the free nucleotide is equal to its total concentration, while the concentrations of all other nucleotide−enzyme complexes are zero.

To obtain the solution of the system of the differential equation, as defined by eq 6, one must first obtain eigenvalues for matrix **M**, then the corresponding eigenvectors. This would involve cumbersome numerical analyses, particularly for the eigenvectors. On the other hand, instead of finding eigenvectors corresponding to the each eigenvalue, λ_i, of matrix **M**, we expand matrix exp(**M***t*) using its eigenvalues, exp($\lambda_l t$), and corresponding projection operators, $\mathbf{Q}_i$, as (*25*, *27*)

$$\exp(\mathbf{M}t) = \sum_{i=0}^{4} \mathbf{Q_i} \exp(\lambda_i t) \qquad (8)$$

The projection operators, $\mathbf{Q}_i$, can easily be analytically defined using the original coefficient matrix **M** and its eigenvalues, λ_i, by Sylvester's theorem (*25*, *27*). A general formula for a projection operator, $\mathbf{Q}_i$, corresponding to an eigenvalue, λ_i, is

$$\mathbf{Q}_i = \frac{\prod_{j \neq i}^{n} (\mathbf{M} - \lambda_j \mathbf{I})}{\prod_{j \neq 1}^{n} (\lambda_i - \lambda_j)} \qquad (9)$$

where n is the number of eigenvalues and **I** is the identity matrix of the same size as **M**.

In the considered case, there are five eigenvalues λ_0, λ_1, λ_2, λ_3, and λ_4. One eigenvalue, $\lambda_0 = 0$, which is the result of the mass conservation in the reaction system, requires that at very long time ($t \rightarrow \infty$) the system approaches equilibrium. Using eq 9, for the considered case of four sequential reactions, one obtains

$$\mathbf{Q}_0 = \frac{(\mathbf{M}-\lambda_1\mathbf{I})(\mathbf{M}-\lambda_2\mathbf{I})(\mathbf{M}-\lambda_3\mathbf{I})(\mathbf{M}-\lambda_4\mathbf{I})}{\lambda_1\lambda_2\lambda_3\lambda_4} \quad (10a)$$

$$\mathbf{Q}_1 = \frac{\mathbf{M}(\mathbf{M}-\lambda_2\mathbf{I})(\mathbf{M}-\lambda_3\mathbf{I})(\mathbf{M}-\lambda_4\mathbf{I})}{\lambda_1(\lambda_1-\lambda_2)(\lambda_1-\lambda_3)(\lambda_1-\lambda_4)} \quad (10b)$$

$$\mathbf{Q}_2 = \frac{\mathbf{M}(\mathbf{M}-\lambda_1\mathbf{I})(\mathbf{M}-\lambda_3\mathbf{I})(\mathbf{M}-\lambda_4\mathbf{I})}{\lambda_2(\lambda_2-\lambda_1)(\lambda_2-\lambda_3)(\lambda_2-\lambda_4)} \quad (10c)$$

$$\mathbf{Q}_3 = \frac{\mathbf{M}(\mathbf{M}-\lambda_1\mathbf{I})(\mathbf{M}-\lambda_2\mathbf{I})(\mathbf{M}-\lambda_4\mathbf{I})}{\lambda_3(\lambda_3-\lambda_1)(\lambda_3-\lambda_2)(\lambda_3-\lambda_4)} \quad (10d)$$

$$\mathbf{Q}_4 = \frac{\mathbf{M}(\mathbf{M}-\lambda_1\mathbf{I})(\mathbf{M}-\lambda_2\mathbf{I})(\mathbf{M}-\lambda_3\mathbf{I})}{\lambda_4(\lambda_4-\lambda_1)(\lambda_4-\lambda_2)(\lambda_4-\lambda_3)} \quad (10e)$$

Application of the matrix projection operators provides the solution for the system of differential eq 4 as

$$\mathbf{N} = \mathbf{Q}_0\mathbf{N}_o + \mathbf{Q}_1\mathbf{N}_o \exp(\lambda_1 t) + \mathbf{Q}_2\mathbf{N}_o \exp(\lambda_2 t) + \mathbf{Q}_3\mathbf{N}_o \exp(\lambda_3 t) + \mathbf{Q}_4\mathbf{N}_o \exp(\lambda_4 t) \quad (11)$$

where $\mathbf{Q}_i$ is defined by eqs 10a−d.

Using projection operators, the numerical analysis of the complex multistep reaction is reduced to finding only the eigenvalues of the original coefficient matrix **M**. The closed-form formulas for the amplitudes of the different normal modes of the reaction are then obtained in terms of rate constants, relaxation times (eigenvalues), and spectroscopic properties of each intermediate.

Equations 9 and 10 show that projection operators, $\mathbf{Q}_i$, are matrices of the same size as the size of the original coefficient matrix **M**. Thus, in general, the products $\mathbf{Q}_i\mathbf{N}_o$ are column vectors, $\mathbf{P}_i$, which are the projections of $\mathbf{N}_o$ on each eigenvector of matrix **M**. The solution of the differential equation system is then

$$\mathbf{N} = \mathbf{P}_0 + \mathbf{P}_1 \exp(\lambda_1 t) + \mathbf{P}_2 \exp(\lambda_2 t) + \mathbf{P}_3 \exp(\lambda_3 t) + \mathbf{P}_4 \exp(\lambda_4 t) \quad (12a)$$

and

$$\begin{pmatrix} N_1 \\ N_2 \\ N_3 \\ N_4 \\ N_5 \end{pmatrix} = \begin{pmatrix} P_{01} \\ P_{02} \\ P_{03} \\ P_{04} \\ P_{05} \end{pmatrix} + \begin{pmatrix} P_{11} \\ P_{12} \\ P_{13} \\ P_{14} \\ P_{15} \end{pmatrix} \exp(\lambda_1 t) + \begin{pmatrix} P_{21} \\ P_{22} \\ P_{23} \\ P_{24} \\ P_{25} \end{pmatrix} \exp(\lambda_2 t) + \begin{pmatrix} P_{31} \\ P_{32} \\ P_{33} \\ P_{34} \\ P_{35} \end{pmatrix} \exp(\lambda_3 t) + \begin{pmatrix} P_{41} \\ P_{42} \\ P_{43} \\ P_{44} \\ P_{45} \end{pmatrix} \exp(\lambda_4 t) \quad (12b)$$

where P_{ij} is the jth element of the projection of the vector of the initial concentrations of $\mathbf{N}_o$ on the eigenvector corresponding to the ith eigenvalue of the matrix **M**. Thus, the solution of the system of the differential equation describing the studied reaction is obtained without directly determining the eigenvectors of **M**. At $t = \infty$ the reaction system reaches equilibrium and the concentrations of all species are described by the elements of vector $\mathbf{P}_0$.

The considered mechanism is complex. There are four normal modes of reaction corresponding to relaxation times $\tau_1 = -1/\lambda_1$, $\tau_2 = -1/\lambda_2$, $\tau_3 = -1/\lambda_3$, and $\tau_4 = -1/\lambda_4$ and four amplitudes, A_1, A_2, A_3, and A_4. The kinetics of nucleotide binding to the DnaB helicase is followed by the fluorescence intensity change of the nucleotide. Thus, each individual amplitude contains a contribution from the fluorescence intensities characterizing nucleotide intermediates of the reaction. In general, each intermediate may have different fluorescence properties. Therefore, there are five molar fluorescence intensities, F_1, F_2, F_3, F_4, and F_5, characterizing N_1, N_2, N_3, N_4, and N_5 states of the nucleotide free and in the complex with the helicase. The total concentration of the nucleotide during the reaction obeys the mass conservation relationship

$$N_{tot} = N_1 + N_2 + N_3 + N_4 + N_5 \quad (13)$$

Therefore, the fluorescence of the system at any time of the reaction, $F(t)$, is defined as

$$F(t) = F_1N_1 + F_2N_2 + F_3N_3 + F_4N_4 + F_5N_5 \quad (14)$$

Introducing eqs 12b and 13 into eq 14 and rearranging provides

$$\mathrm{F}(t) = \mathrm{F}_1\mathrm{N}_1 + \begin{pmatrix} F_2P_{02} + F_3P_{03} + F_4P_{04} + F_5P_{05} \\ F_2P_{12} + F_3P_{13} + F_4P_{14} + F_5P_{15} \\ F_2P_{22} + F_3P_{23} + F_4P_{24} + F_5P_{25} \\ F_2P_{32} + F_3P_{33} + F_4P_{34} + F_5P_{35} \\ F_2P_{42} + F_3P_{43} + F_4P_{44} + F_5P_{45} \end{pmatrix}^T \begin{pmatrix} 1 \\ \exp(\lambda_1 t) \\ \exp(\lambda_2 t) \\ \exp(\lambda_3 t) \\ \exp(\lambda_4 t) \end{pmatrix} \quad (15)$$

where index T indicates the transpose matrix.

The experimentally determined total amplitude, A_{tot}, of a stopped-flow trace is defined as

$$A_{tot} = F(0) - F(\infty) \quad (16)$$

where $F(0)$ and $F(\infty)$ are the observed fluorescence intensities, $F(t)$, of the system at $t = 0$ and $t = \infty$, respectively. Introducing $t = 0$ for $F(0)$ and $t = \infty$ for $F(\infty)$ into eq 15 provides

$$F(0) = F_1N_{tot} + \begin{pmatrix} P_{02} + P_{12} + P_{22} + P_{32} + P_{42} \\ P_{03} + P_{13} + P_{23} + P_{33} + P_{43} \\ P_{04} + P_{14} + P_{24} + P_{34} + P_{44} \\ P_{05} + P_{15} + P_{25} + P_{35} + P_{45} \end{pmatrix}^T \begin{pmatrix} F_2 - F_1 \\ F_3 - F_1 \\ F_4 - F_1 \\ F_5 - F_1 \end{pmatrix} \quad (17)$$

and

$$F(\infty) = F_1N_{tot} + (P_{02}\ \ P_{03}\ \ P_{04}\ \ P_{05}) \begin{pmatrix} F_2 - F_1 \\ F_3 - F_1 \\ F_4 - F_1 \\ F_5 - F_1 \end{pmatrix} \quad (18)$$

Subtracting eq 18 from 17 gives the total amplitude as

$$A_{tot} = \begin{pmatrix} P_{12} + P_{13} + P_{14} + P_{15} \\ P_{22} + P_{23} + P_{24} + P_{25} \\ P_{32} + P_{33} + P_{34} + P_{35} \\ P_{42} + P_{43} + P_{44} + P_{45} \end{pmatrix}^T \begin{pmatrix} F_2 - F_1 \\ F_3 - F_1 \\ F_4 - F_1 \\ F_5 - F_1 \end{pmatrix} \quad (19)$$

Because, the total amplitude, A_{tot}, of the stopped-flow trace is the sum of the individual amplitudes of all normal modes,

$$A_{tot} = A_1 + A_2 + A_3 + A_4 \quad (20)$$

the individual amplitudes A_1, A_2, A_3, and A_4 for each normal mode of the reaction are then

$$A_1 = (P_{12}\ \ P_{13}\ \ P_{14}\ \ P_{15}) \begin{pmatrix} F_2 - F_1 \\ F_3 - F_1 \\ F_4 - F_1 \\ F_5 - F_1 \end{pmatrix} \quad (21)$$

$$A_2 = (P_{22}\ \ P_{23}\ \ P_{24}\ \ P_{25}) \begin{pmatrix} F_2 - F_1 \\ F_3 - F_1 \\ F_4 - F_1 \\ F_5 - F_1 \end{pmatrix} \quad (22)$$

$$A_3 = (P_{32}\ \ P_{33}\ \ P_{34}\ \ P_{35}) \begin{pmatrix} F_2 - F_1 \\ F_3 - F_1 \\ F_4 - F_1 \\ F_5 - F_1 \end{pmatrix} \quad (23)$$

$$A_4 = (P_{42}\ \ P_{43}\ \ P_{44}\ \ P_{45}) \begin{pmatrix} F_2 - F_1 \\ F_3 - F_1 \\ F_4 - F_1 \\ F_5 - F_1 \end{pmatrix} \quad (24)$$

Equations 20−24 are closed-form, explicit expressions for the total and individual amplitudes for the sequential, four-step reaction mechanism of nucleotide binding to the DnaB helicase, described by eq 2. Notice, once the matrix projection operators are formulated in terms of the original coefficient matrix **M**, the total and individual amplitudes of the reaction system can be explicitly defined in terms of rate constants, relaxation times, and spectroscopic properties of the intermediates. The closed-form expressions for the individual amplitudes of all kinetic steps enable one to extract the spectroscopic properties of each intermediate of the reaction, thus, providing information about the structures of the intermediates, unavailable by any other methods. Because the fluorescence of the free nucleotide, F_1, can be set as 1, only the values of the remaining four molar fluorescence intensities, F_2, F_3, F_4, and F_5, relative to F_1, have to be determined. Notice, F_2, F_3, F_4, and F_5 are uniquely determined, relative to F_1, by eqs 20−24. However, in practice, due to experimental error, determination of F_2, F_3, F_4, and F_5 can be achieved through nonlinear least-squares fitting of the experimentally obtained individual amplitudes, as described below. Extension of the analysis to more complex reaction systems is straightforward.

Relaxation Times. Examination of the relaxation times of the studied kinetics, as a function of ligand concentration, constitutes the first and fundamental step in establishing the mechanism of the complex reaction and the rate constants of particular elementary processes (*26*). The reciprocal relaxation times for the four-step sequential reaction, described by eq 2, as a function of the free macromolecule concentration, are shown in Figure 1. Relaxation times have been obtained by direct, numerical determination of the eigenvalues, λ_1, λ_2, λ_3, and λ_4, of matrix **M** at a given free macromolecule concentration, H, using the identities of $1/\tau_1 = -\lambda_1$, $1/\tau_2 = -\lambda_2$, $1/\tau_3 = -\lambda_3$, and $1/\tau_4 = -\lambda_4$. Because of the large differences between the values of the selected rate constants among the elementary steps, the relaxation times differ significantly at any concentration of the macromolecule, i.e., the normal modes of the reaction are close to the "uncoupled" ones (*26*). In such a situation, it could be possible to obtain approximate formulas for each of the relaxation times; however, the numerical approach applied here avoids such approximations. The largest reciprocal relaxation time has typical characteristics of the bimolecular binding process with $1/\tau_1$ increasing linearly with the macromolecule concentration in the high macromolecule concentration range (*26*). On the other hand, at low macromolecule concentrations, there is clearly a nonlinear region (Figure 1). This experimentally observed region (see below) is only evident because no approximate expressions for this relaxation time have been used. The reciprocal relaxation times $1/\tau_2$, $1/\tau_3$, and $1/\tau$, for the considered sequential four-step reaction, show hyperbolic dependence upon the [macromolecule] reaching plateau values at the higher [macromolecule]. As a result, $1/\tau_2$, $1/\tau_3$, and $1/\tau_4$ become independent of the macromolecule concentration in the higher concentration range.

Amplitudes. Analysis of the amplitudes of the spectroscopic relaxation process provides an additional test of the determined mechanism and offers a unique opportunity to obtain information about the structure of the reaction intermediates and the physical nature of the elementary steps. The dependence of individual amplitudes, A_1, A_2, A_3, and A_4, expressed as fractions of the total amplitude, A_{tot}, ($A_i/\sum A_i$) upon the macromolecule concentration, for the considered sequential reaction, is shown in Figure 2. The computer simulations have been performed using eqs 21−24. The selected molar fluorescence intensities are $F_2 = 5$, $F_3 = 5$, $F_4 = 5$, and $F_5 = 5$; rate constants are the same as in Figure 1. It is clear that at low macromolecule concentrations predominantly the amplitudes of the fourth A_4 and third A_3 normal modes of the reaction contribute significantly to the observed A_{tot}, although the major fluorescence change, as compared to the fluorescence of the free ligand, accompanies the formation of N_2. Such behavior is the result of the low efficiency of the N_2 complex formation at a low [macromolecule], while the formed complex still relaxes with the third and fourth normal modes. At high macromolecule concentrations, the amplitude of the first normal mode, A_1, dominates the relaxation process. The computer simulations in Figure 2 show that all four amplitudes of the present relaxation steps are detectable, although there is no additional fluorescence change in the transition from N_2 to all subsequent intermediates. As mentioned above, this is evident from eqs 20−24, which show that the amplitude for a given normal mode of the reaction is mainly affected by the values of relaxation times, rate constants, and the differences between

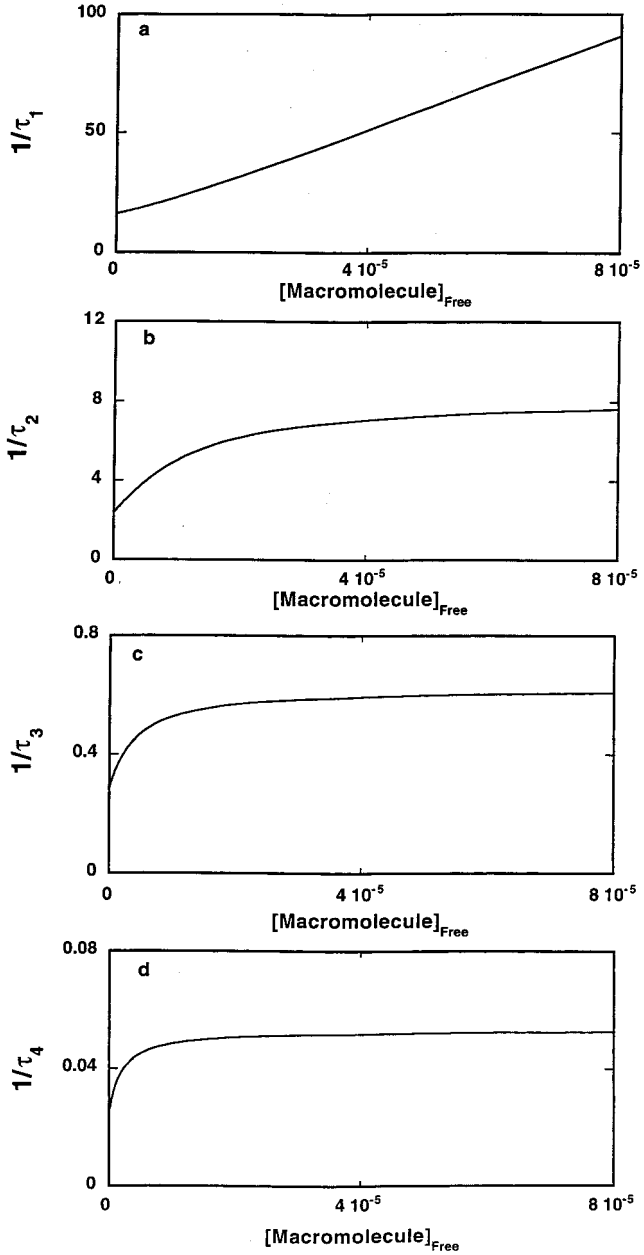

FIGURE 1: Computer simulation of the dependence of reciprocal relaxation times for the four-step sequential mechanism of ligand binding to a single, independent site on a macromolecule, defined by eq 2, upon free macromolecule concentration. Relaxation times have been obtained by numerically determining the eigenvalues of the coefficient matrix **M** (λ_1, λ_2, λ_3, λ_4), then using identities $1/\tau_1 = -\lambda_1$, $1/\tau_2 = -\lambda_2$, $1/\tau_3 = -\lambda_3$, and $1/\tau_4 = -\lambda_4$. The simulations have been performed using rate constants $k_1 = 1 \times 10^6$ M^{-1} s^{-1}, $k_{-1} = 10$ s^{-1}, $k_2 = 5$ s^{-1}, $k_{-2} = 3$ s^{-1}, $k_3 = 0.5$ s^{-1}, $k_{-3} = 0.3$ s^{-1}, $k_4 = 0.05$ s^{-1}, and $k_{-4} = 0.03$ s^{-1}. The selected total ligand, N_{tot}, concentration is 1×10^{-8} M; (a) $1/\tau_1$, (b) $1/\tau_2$, (c) $1/\tau_3$, (d) $1/\tau_4$.

thespectroscopic properties of the intermediates and the free ligand (see above).

Computer simulations shown in Figure 2 were performed with given values of the relative fluorescence intensities for all intermediates. In experimental studies of a kinetic system, this process is reversed, i.e., from the dependence of the amplitudes of the system upon macromolecule (or ligand) concentrations one can determine the spectroscopic parameters characterizing all intermediates. Below we discuss the approach as applied for the case of nucleotide association with the DnaB helicase.

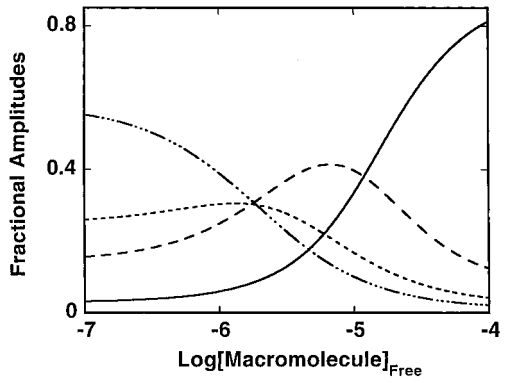

FIGURE 2: Computer simulation of the dependence of fractional individual A_1, A_2, A_3, and A_4 relaxation amplitudes for the four-step sequential mechanism of ligand binding to a single, independent site on a macromolecule, defined by eq 2, upon the logarithm of the free macromolecule concentration. The relative fluorescence intensities, F_2, F_3, F_4, and F_5, characterizing corresponding intermediates, N_2, N_3, N_4, and N_5 are 5, 5.5, 5.5, and 5.5, respectively. The fluorescence of the free ligand, N_1, is taken as 1. The individual amplitudes are expressed as fractions of the total amplitude. The simulations have been performed using closed-form expressions defined by eqs 21−24 with the rate constants $k_1 = 1 \times 10^6$ M^{-1} s^{-1}, $k_{-1} = 10$ s^{-1}, $k_2 = 5$ s^{-1}, $k_{-2} = 3$ s^{-1}, $k_3 = 0.5$ s^{-1}, $k_{-3} = 0.3$ s^{-1}, $k_4 = 0.05$ s^{-1}, and $k_{-4} = 0.03$ s^{-1}; A_1 (—), A_2 (− − −), A_3 (---), A_4 (−•••−).

RESULTS

Binding of the Fluorescent Nucleotide Analogues, MANT-AMP-PNP and MANT-ADP, to a Single, Noninteracting Site on the DnaB Helicase. Quantitative fluorescence titrations show that there are six nucleotide-binding sites on the DnaB hexamer and the binding process is biphasic, resulting from the negative cooperative interactions among binding sites (*19*−*22*). Biphasic binding results from the fact that negative cooperativity is limited to the adjacent subunits. As a result, the first three nucleotide molecules bind to three noninteracting sites (*19*−*22*). In the first step, we addressed the mechanism of nucleotide binding to a single, noninteracting site on the DnaB protein hexamer. Fluorescence titrations ($\lambda_{ex} = 295$ nm, $\lambda_{em} = 450$ nm) of MANT-AMP-PNP and MANT-ADP, with the DnaB helicase in buffer T2 (pH 8.1, 100 mM NaCl, 20 °C), are shown in Figure 3. The concentrations of the nucleotides are 1.5×10^{-7} M. Because the excitation wavelength applied is at 295 nm, the excitation of the nucleotide analogue is minimal and the increase of the nucleotide fluorescence originates predominantly through energy transfer from the protein tryptophans. We previously determined that all tryptophan residues of the DnaB helicase are clustered around the nucleotide-binding site of the enzyme (*20*). With the excitation at the tryptophan absorption band, the maximum relative fluorescence increase of MANT-AMP-PNP and MANT-ADP are ∼13- and ∼17-fold, respectively (Figure 3, Table 1). Analogous titrations, using the excitation directly in the MANT absorption maximum ($\lambda_{ex} = 356$ nm), produce only ∼3-fold increase of the MANT-derivative fluorescence upon saturation with the DnaB helicase (*21*).

The concentration of the nucleotides (1.5×10^{-7} M) has been selected to ensure that, over the entire isotherm, only association with one of the six binding sites on the hexamer is observed (*19*−*22*). The solid lines in Figure 3 are computer

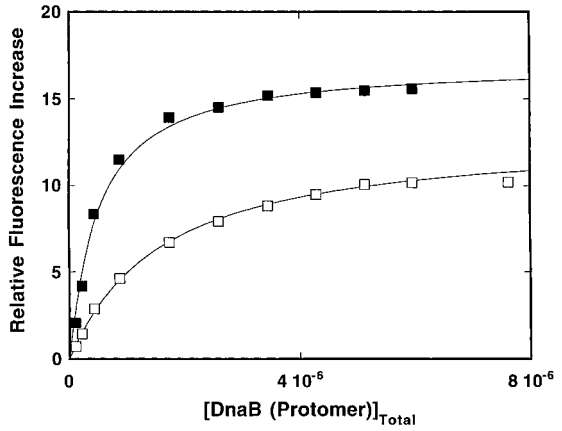

FIGURE 3: Fluorescence titrations of MANT-AMP-PNP and MANT-ADP with the DnaB helicase in buffer T2 (pH 8.1, 100 mM NaCl, 20 °C), MANT-AMP-PNP (□), and MANT-ADP (■). The solid lines are the best fits of the experimental isotherms to a single site isotherm (eq 25), using the intrinsic binding constant $K = 6.5 \times 10^5$ M^{-1} and 2.3×10^6 M^{-1} for MANT-AMP-PNP and MANT ADP, respectively (see text for details). Concentrations of both nucleotides are 1.5×10^{-7} M.

fits using a single-site binding isotherm

$$\Delta F = \frac{\Delta F_{max} K[\mathrm{H}]}{1 + K[\mathrm{H}]} \qquad (25)$$

where K is the intrinsic binding constant, ΔF_{max} is the maximum fluorescence increase of the nucleotide saturated with the enzyme, and [H] is the concentration of the DnaB helicase (Protomer). The obtained values are $K = (6.5 \pm 1) \times 10^5$ M^{-1}, $\Delta F_{max} = 13$, and $K = (2.3 \pm 0.5) \times 10^6$ M^{-1}, $\Delta F_{max} = 17$ for MANT-AMP-PNP and MANT-ADP, respectively (Table 1). The obtained values of the intrinsic constants are in excellent agreement with the values previously obtained, using protein fluorescence to monitor the nucleotide binding and analyzing the entire binding isotherm with the statistical thermodynamic model for the protein hexamer (hexagon model) (*19*−*22*). Notice, the increase of the relative fluorescence is larger in the case of MANT-ADP than MANT-AMP-PNP, indicating that the MANT moiety of ADP is closer to the protein tryptophans in the binding site than the MANT group of the AMP-PNP analogue. These data indicate that the conformational state of the ADP analogue in the binding site is different from that of the AMP-PNP (see below).

Kinetics of the Ribose-Modified Fluorescent ATP Analogue, MANT-AMP-PNP, Binding to a Single, Noninteracting Site on the DnaB Helicase. Stopped-flow experiments were performed under pseudo-first-order conditions by mixing the nucleotide with a large excess of the DnaB helicase. At all concentrations used, the DnaB helicase fully preserved its hexameric structure (*6*, *7*). The stopped-flow kinetic trace of the MANT-AMP-PNP fluorescence, after mixing 3×10^{-7} M analogue with 1.2×10^{-5} M DnaB helicase (Protomer) (final concentrations) in buffer T2 (pH 8.1, 100 mM NaCl, 20 °C), is shown in Figure 4. The curve has been recorded in two time bases, 1 and 200 s. The observed kinetics is very complex, clearly showing the presence of multiple steps. The solid line in Figure 4 is a nonlinear least-squares fit of the experimental curve using the four-exponential fit. As indicated by the included deviations of the experimental curve from the fit, the three-exponential function does not provide an adequate description of the experimentally observed kinetics. Thus, the four-exponential fit is necessary to represent the observed experimental curve. A higher number of exponents does not significantly improve the statistics of the fit. Therefore, the association of MANT-AMP with the DnaB helicase is at least a four-step process.

The reciprocal relaxation times, $1/\tau_1$, $1/\tau_2$ $1/\tau_3$, and $1/\tau_4$, characterizing the four binding steps, as a function of the DnaB helicase concentration (Protomer) are shown in Figure 5. The relaxation times strongly differ in their values, indicating that the observed kinetic steps are close to the "uncoupled" ones (*26*). The largest reciprocal relaxation time, $1/\tau_1$, increases with the [DnaB], and the dependence becomes linear at high enzyme concentrations, although there is a nonlinear phase at the low [DnaB]. Such behavior is typical for the relaxation time characterizing the bimolecular-binding step (Figure 1). On the other hand, $1/\tau_2$ and $1/\tau_3$ show hyperbolic dependence upon the [DnaB], while $1/\tau_4$ is, within experimental accuracy, independent of helicase concentrations. The simplest minimum mechanism that can account for the observed dependence of the relaxation times upon the enzyme concentration is a four-step, sequential binding process in which bimolecular association is followed by three isomerization steps as described by Scheme 1.

The solid lines in Figure 5 are computer fits of the relaxation times according to the above mechanism. The analysis was first performed by numerical, nonlinear least-squares fitting of the individual relaxation times, then the values of the rate constants were refined by global fitting, which simultaneously includes all relaxation times. The obtained rate constants for the mechanism defined by Scheme 1 are $k_1 = (9 \pm 1.5) \times 10^5$ M^{-1} s^{-1}, $k_{-1} = 5 \pm 1.2$ s^{-1}, $k_2 = 6 \pm 2$ s^{-1}, $k_{-2} = 5 \pm 1.5$ s^{-1}, $k_3 = 0.3 \pm 0.1$ s^{-1}, $k_{-3} = 0.7 \pm 0.2$ s^{-1}, $k_4 = 0.011 \pm 0.004$ s^{-1}, and $k_{-4} = 0.011 \pm 0.004$ s^{-1} (Table 2).

The equilibrium association binding constants for each step in Scheme 1 are $K_1 = k_1/k_{-1}$, $K_2 = k_2/k_{-2}$, $K_3 = k_3/k_{-3}$, and $K_4 = k_4/k_{-4}$. Introducing the values of the rate constants provides $K_1 = (1.8 \pm 0.6) \times 10^5$ M^{-1}, $K_2 = 1.3 \pm 0.4$, $K_3 = 0.4 \pm 0.12$, and $K_4 = 1 \pm 0.3$. It is clear that the first step has a dominant contribution to the free energy of the nucleotide binding. Within experimental error, the second and fourth steps do not contribute to the energetics of binding, while the third step is even energetically unfavorable. The overall binding constant K is related to the partial equilibrium steps by

$$K = K_1 (1 + K_2 + K_2 K_3 + K_2 K_3 K_4) \qquad (26)$$

Introducing the values of equilibrium constants for partial equilibrium steps into eq 26 gives $K = (6.3 \pm 1.4) \times 10^5$ M^{-1}. This value is, within experimental accuracy, in excellent agreement with the intrinsic binding constant $K = (6.5 \pm 1) \times 10^5$ M^{-1} determined by equilibrium titration (Figure 4, Table 1).

Individual Amplitudes of Relaxation Steps in MANT-AMP-PNP Binding to the DnaB Hexamer. The dependence of the individual amplitudes, A_1, A_2, A_3, and A_4 of all four relaxation

Table 1: Intrinsic Binding Constant, K_1, and Maximum Fluorescence Increase ΔF_{max} for Binding of the Ribose- and Base-Modified Fluorescent ATP and ADP Analogues, MANT-AMP-PNP, MANT-ADP, ϵAMP-PNP, and ϵADP to a Single, Noninteracting Nucleotide-Binding Site on the DnaB Hexamer[a]

	MANT-AMP-PNP	MANT-ADP	ϵAMP-PNP	ϵADP
K (M^{-1})	$(6.5 \pm 1) \times 10^5$	$(2.3 \pm 0.5) \times 10^6$	$(6 \pm 1) \times 10^4$	$(3.3 \pm 0.7) \times 10^5$
ΔF_{max}	13 ± 1	17 ± 2	2.7 ± 0.3	3.4 ± 0.3

[a] MANT-analogues, $\lambda_{ex} = 295$ mm; $\lambda_{em} = 450$ mm. Etheno-analogues, $\lambda_{ex} = 325$ mm; $\lambda_{em} = 410$ mm. The binding isotherms have been obtained in buffer T2 (pH 8.1, 100 mM NaCl, 20 °C) for the MANT-analogues and in the same buffer containing 100 mM acrylamide for the etheno-analogues (see text for details).

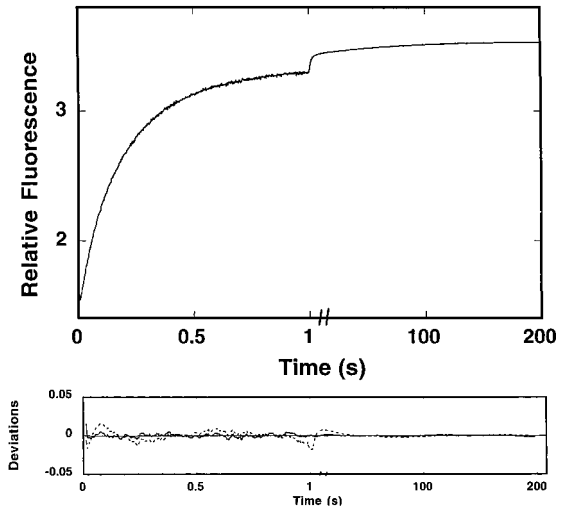

FIGURE 4: Top panel is the fluorescence stopped-flow kinetic trace, recorded in two time bases, 1 and 200 s, after mixing the DnaB helicase with MANT-AMP-PNP in buffer T2 (pH 8.1, 100 NaCl, 20 °C) ($\lambda_{ex} = 295$ nm, $\lambda_{em} > 400$ nm). The final concentrations of the DnaB helicase and the nucleotide are 1.2×10^{-5} M (Protomer) and 3×10^{-7} M, respectively. The solid line is the four-exponential, nonlinear least-squares fit of the experimental curve using eq 1. The lower panel shows the deviations of the experimental curve from the fit using a three-exponential (---) and a four-exponential (—) function, respectively (equation 1).

steps upon the logarithm of the DnaB protein concentration (Protomer) are shown in Figure 6. The individual amplitudes are expressed as a fraction of the total amplitude, $A_i/\sum A_i$. At low helicase concentrations, the amplitude of the first bimolecular process does not significantly contribute to the observed kinetics. The total amplitude is dominated by the second relaxation process (amplitude A_2), which constitutes ~60% of the observed fluorescence increase. The amplitudes A_3 and A_4 of the third and fourth relaxation steps contribute to the observed kinetics mainly at low enzyme concentrations. As the concentration of the DnaB helicase increases, the amplitude of the bimolecular step, A_1, increases and at high enzyme concentrations becomes a dominant relaxation effect (Figure 6).

Such behavior of the individual amplitudes is in full agreement with the proposed sequential mechanism (Scheme 1) deduced from the relaxation time analysis. Using the matrix projection operator technique, described above, we can determine molar fluorescence intensities characterizing each intermediate of the reaction relative to the fluorescence of the free nucleotide, i.e., we can assess the conformational state of the enzyme−nucleotide complex. It should be pointed out that the maximum increase of the fluorescence of MANT-AMP-PNP saturated with the DnaB helicase is independently known ($\Delta F_{max} = 13$) from the equilibrium fluorescence titrations (Figure 3). Also, at saturating concentrations of the

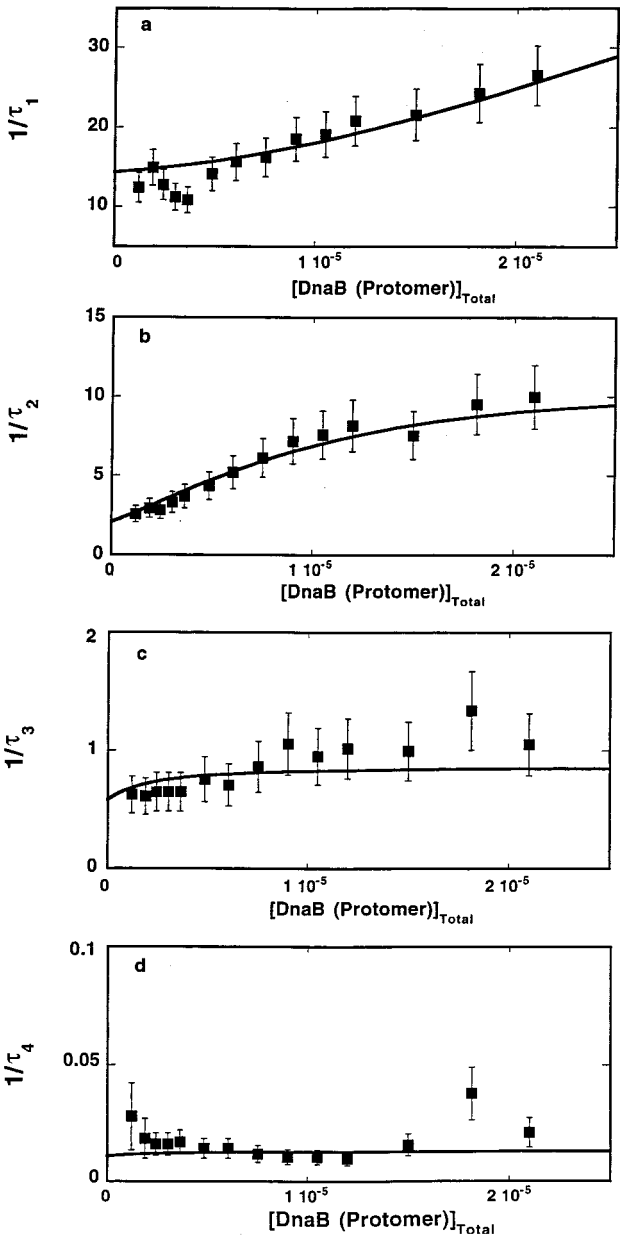

FIGURE 5: Dependence of the reciprocal of the relaxation times for the binding of MANT-AMP-PNP to the DnaB helicase in buffer T2 (pH 8.1, 100 mM NaCl, 20 °C) upon the total concentration of the enzyme (Protomer). The solid lines are nonlinear least-squares fits of the experimental data to the four-step sequential mechanism, defined by eq 2, using rate constants $k_1 = 9 \times 10^5$ M^{-1} s^{-1}, $k_{-1} = 5$ s^{-1}, $k_2 = 6$ s^{-1}, $k_{-2} = 5$ s^{-1}, $k_3 = 0.3$ s^{-1}, $k_{-3} = 0.7$ s^{-1}, $k_4 = 0.011$ s^{-1}, and $k_{-4} = 0.011$ s^{-1} (Table 2); (a)$1/\tau_1$, (b) $1/\tau_2$, (c) $1/\tau_3$, (d) $1/\tau_4$. The error bars are standard deviations obtained from three to four independent experiments.

helicase, ΔF_{max} can be analytically expressed as a function of the partial equilibrium binding constants and molar

Scheme 1

$$\text{Helicase} + \text{N} \underset{k_{-1}}{\overset{k_1}{\Leftrightarrow}} (\text{H}-\text{N})_1 \underset{k_{-2}}{\overset{k_2}{\Leftrightarrow}} (\text{H}-\text{N})_2 \underset{k_{-3}}{\overset{k_3}{\Leftrightarrow}} (\text{H}-\text{N})_3 \underset{k_{-4}}{\overset{k_4}{\Leftrightarrow}} (\text{H}-\text{N})_4$$

Table 2: Kinetic, Thermodynamic, and Spectroscopic Parameters Characterizing the Binding of Ribose- and Base-Modified Fluorescent ATP and ADP Analogues, MANT-AMP-PNP, MANT-ADP, ϵAMP-PNP, and ϵADP to a Single, Noninteracting Site on the DnaB Hexamer Helicase (see text for details)

	MANT-AMP-PNP	MANT-ADP	ϵAMP-PNP	ϵADP
k_1 ($M^{-1}s^{-1}$)	$(9 \pm 1.5) \times 10^5$	$(3.5 \pm 1) \times 10^6$	$(3.4 \pm 1) \times 10^5$	$(2.6 \pm 0.6) \times 10^6$
k_{-1} (s^{-1})	5 ± 1.2	9 ± 2	16 ± 2	10 ± 2
k_2 (s^{-1})	6 ± 2	14 ± 2	3.3 ± 0.8	4 ± 1
k_{-2} (s^{-1})	5 ± 1.5	6 ± 1	8 ± 2	6.5 ± 1.5
k_3 (s^{-1})	0.3 ± 0.1	0.6 ± 0.25	0.05 ± 0.02	0.01 ± 0.003
k_{-3} (s^{-1})	0.7 ± 0.2	1.8 ± 0.6	0.07 ± 0.02	0.07 ± 0.03
k_4 (s^{-1})	0.011 ± 0.004	0.003 ± 0.0015	0.01 ± 0.004	0.009 ± 0.004
k_{-4} (s^{-1})	0.011 ± 0.004	0.005 ± 0.002	0.0045 ± 0.002	0.0045 ± 0.002
K_1 (M^{-1})	$(1.8 \pm 0.6) \times 10^5$	$(4.4 \pm 1) \times 10^5$	$(2.1 \pm 0.7) \times 10^4$	$(2.6 \pm 0.7) \times 10^5$
K_2	1.3 ± 0.4	2.3 ± 0.7	0.4 ± 0.12	0.6 ± 0.2
K_3	0.4 ± 0.12	0.3 ± 0.1	0.7 ± 0.25	0.15 ± 0.05
K_4	1 ± 0.3	0.6 ± 0.2	2.2 ± 0.6	2 ± 0.6
overall binding constant (M^{-1})	$(6.3 \pm 1.4) \times 10^5$	$(2.0 \pm 0.6) \times 10^6$	$(5 \pm 1.5) \times 10^4$	$(4.8 \pm 1.2) \times 10^5$
ΔF_2	13.6 ± 1.2	16.6 ± 1.5	5.3 ± 1	4.6 ± 0.7
ΔF_3	11.9 ± 1	14.2 ± 1.5	4.3 ± 1	4.9 ± 0.7
ΔF_4	12 ± 1.5	14.2 ± 2	1.8 ± 0.6	2.5 ± 0.6
ΔF_5	12.7 ± 2	35.5 ± 5	3.7 ± 1	1.1 ± 0.3

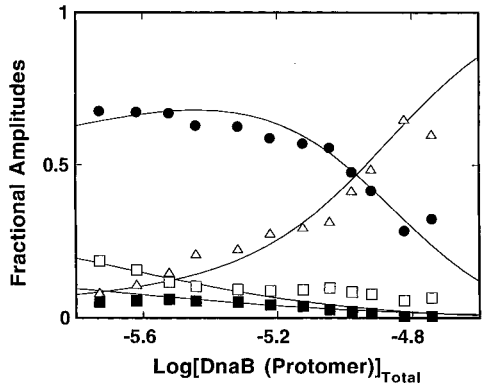

FIGURE 6: Dependence of the individual relaxation amplitudes of the kinetic process of MANT-AMP-PNP binding to the DnaB helicase in buffer T2 (pH 8.1, 100 mM NaCl, 20 °C) upon the logarithm of the total concentration of the enzyme (Protomer). The solid lines are computer fits according to the four-step sequential mechanism using eqs 21−24, with the relative fluorescence intensities $\Delta F_2 = 13.6$, $\Delta F_3 = 11.9$, $\Delta F_4 = 12$, and $\Delta F_5 = 12.7$. The fluorescence intensity of the free MANT-AMP-PNP is taken as $\Delta F_1 = 1$. The maximum fluorescence increase of the nucleotide has been determined in the equilibrium fluorescence titration as $\Delta F_{max} = 13$ (Figure 3). The rate constants are the same as those obtained from the relaxation time analysis (Table 2); A_1 (△), A_2 (●), A_3 (□), A_4 (■).

fluorescence intensities of each intermediate as

$$\Delta F_{max} = \frac{\Delta F_2}{1 + K_2 + K_2K_3 + K_2K_3K_4} + \frac{K_2\Delta F_3}{1 + K_2 + K_2K_3 + K_2K_3K_4} + \frac{K_2K_3\Delta F_4}{1 + K_2 + K_2K_3 + K_2K_3K_4} + \frac{K_2K_3K_4\Delta F_5}{1 + K_2 + K_2K_3 + K_2K_3K_4} \quad (27)$$

where ΔF_2, ΔF_3, ΔF_4, and ΔF_5 are molar fluorescence intensities of each intermediate of the DnaB helicase−nucleotide cofactor complex, relative to the fluorescence of the free nucleotide, ΔF_1. Equation 27 constitutes an additional relationship among partial equilibrium constants and the fluorescence parameters characterizing the intermediates. Because the individual amplitudes are analyzed as fractions of the total amplitudes, the value of ΔF_{max} plays the role of a scaling factor. Thus, ΔF_{max} affects only the absolute values of the determined molar fluorescence intensities, but not their relative values with respect to each other. The solid lines in Figure 6 are computer fits of the experimentally determined fractional individual amplitudes ($A_i/\sum A_i$) of the reaction using eqs 20−24 and 27. The applied fitting procedure was the same as the one used for the relaxation times (see above). First, eqs 21−24 were fitted to the individual amplitudes using the same rate constants as obtained from the examination of the relaxation times or by allowing the rate constants to float between ±10% of the values determined in the relaxation time analysis. Both approaches provide similar values of the relative fluorescence intensities. In the final step, global fitting with simultaneous fitting of all four individual amplitudes refined the obtained spectroscopic parameters. In these calculations, the fluorescence of the free MANT-AMP-PNP was taken as $\Delta F_1 = 1$. The data indicate that the largest relative fluorescence change, as compared to the free AMP-PNP analogue, occurs in the first binding step, i.e., in the formation of the $(H-N)_1$. Upon formation of this complex, the fluorescence of the nucleotide increases by a factor of 13.6 ($\Delta F_2 = 13.6 \pm 1.2$) as compared to the free MANT-AMP-PNP. However, formation of subsequent intermediates is accompanied by lower fluorescence increases than the ΔF_1 with $\Delta F_3 = 11.9 \pm 1$, $\Delta F_4 = 12 \pm 1$, and $\Delta F_5 = 12.7 \pm 1.5$ (Table 2). These results suggest that in the initial binding step the MANT group is closer to the protein tryptophans than in the subsequent intermediates (see Discussion).

Kinetics of Binding the Ribose-Modified Fluorescent ADP Analogue, MANT-ADP, to a Single Noninteracting Site on the DnaB Helicase. The stopped-flow kinetic experiments for the binding of MANT-ADP to the DnaB helicase have been performed in the same way as described above for MANT-AMP-PNP. The observed kinetic curves can only

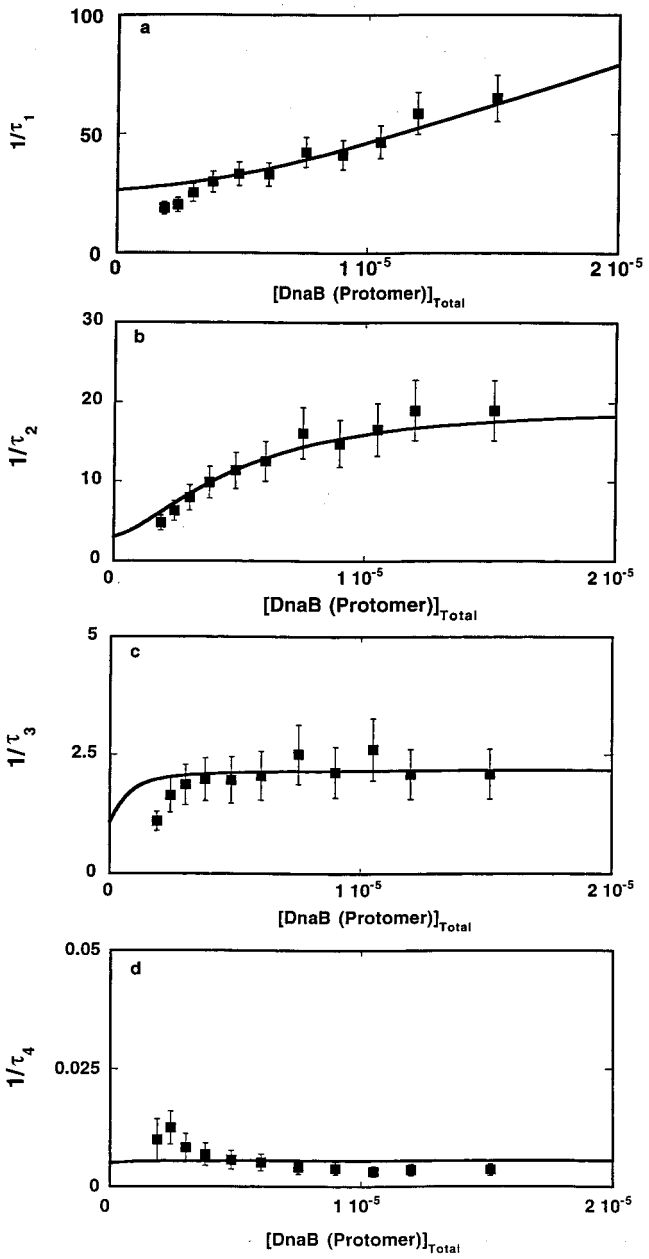

FIGURE 7: Dependence of the reciprocal of the relaxation times for the binding of MANT-ADP to the DnaB helicase in buffer T2 (pH 8.1, 100 mM NaCl, 20 °C) upon the total concentration of the helicase (Protomer). The solid lines are nonlinear least-squares fits according to the four-step sequential mechanism, defined by eq 2, with the rate constants $k_1 = 3.5 \times 10^6$ M^{-1} s^{-1}, $k_{-1} = 9$ s^{-1}, $k_2 = 14$ s^{-1}, $k_{-2} = 6$ s^{-1}, $k_3 = 0.6$ s^{-1}, $k_{-3} = 1.8$ s^{-1}, $k_4 = 0.003$ s^{-1}, and $k_{-4} = 0.005$ s^{-1}; (a) $1/\tau_1$, (b) $1/\tau_2$, (c) $1/\tau_3$, (d) $1/\tau_4$. The error bars are standard deviations obtained from three to four independent experiments.

be adequately described by a four-exponential function, not by a three-exponential function (data not shown). Thus, similar to MANT-AMP-PNP, the association of the ADP analogue with the single, noninteracting binding site of the DnaB helicase includes at least four steps.

The reciprocal relaxation times, $1/\tau_1$, $1/\tau_2$, $1/\tau_3$, and $1/\tau_4$, characterizing the four-step kinetic processes, as a function of the total DnaB helicase concentration (Protomer), are shown in Figure 7. The largest reciprocal relaxation time, $1/\tau_1$, increases with the [DnaB] as expected for the relaxation time characterizing the bimolecular binding step (see Figure 1), while $1/\tau_2$, $1/\tau_3$, and $1/\tau_4$ reach plateaus at high enzyme

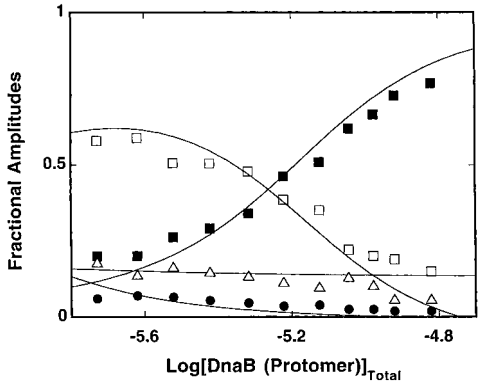

FIGURE 8: Dependence of the individual relaxation amplitudes of the kinetic process of MANT-ADP binding to the DnaB helicase in buffer T2 (pH 8.1, 100 mM NaCl, 20 °C) upon the logarithm of the total concentration of the enzyme (Protomer). The solid lines are computer fits according to the four-step sequential mechanism using eqs 21−24, with the relative fluorescence intensities $\Delta F_2 = 16.6$, $\Delta F_3 = 14.2$, $\Delta F_4 = 14.2$, and $\Delta F_5 = 35.5$. The fluorescence intensity of the free MANT-ADP is taken as $\Delta F_1 = 1$. The maximum fractional fluorescence increase of the nucleotide has been determined in the equilibrium fluorescence titration as $\Delta F_{max} = 17$ (Figure 3). The rate constants are the same as obtained from the relaxation time analysis (Table 2); A_1 (■), A_2 (□), A_3 (●), A_4 (△).

concentrations. Therefore, the association of the ADP analogue with the single, noninteracting nucleotide-binding site can be described by the same mechanism as determined for the AMP-PNP analogue in which the bimolecular association is followed by three conformational transitions of the formed complex (Scheme 1).

The solid lines in Figure 7 are computer fits of the relaxation times according to the four-step mechanism (Scheme 1) with the rate constants included in Table 2. The data show that the values of all rate constants are considerably different, even though the binding mechanism of the MANT-ADP binding is the same as determined for MANT-AMP-PNP. Thus, both k_1 and k_{-1}, characterizing the bimolecular binding process, are by factors of ∼4 and ∼2 higher than in the case of the AMP-PNP analogue. Also, the fourth process is significantly slower than the one observed for AMP-PNP.

The differences between rate constants are reflected in the energetics of the partial steps of the reaction (Table 2). The first binding step is energetically much more favorable than the corresponding step for MANT-AMP-PNP and dominates the energetics of MANT-ADP binding. The first and second steps contribute to the increased affinity of the nucleotide, while the third and fourth steps have a decreasing effect on the affinity. The overall binding constant K (eq 26) is $(2.0 \pm 0.6) \times 10^6$ M^{-1}, as compared to $(2.3 \pm 0.4) \times 10^6$ M^{-1} determined in equilibrium fluorescence titrations (Figure 3). This value is significantly higher than the value of the overall binding constant observed for AMP-PNP (Table 1), which is in agreement with equilibrium studies showing that the ADP analogues have a higher affinity than the ATP analogues (*19*−*22*).

The dependence of the fractional individual amplitudes, A_1, A_2, A_3, and A_4, of all four relaxation steps upon the logarithm of the total DnaB concentration (Protomer), is shown in Figure 8. Molar fluorescence intensities, of each intermediate of the reaction, relative to the molar fluorescence

of the free MANT-ADP, have been obtained using the matrix projection operator technique described above. The maximum fractional increase of the MANT-ADP fluorescence, upon saturation with the DnaB helicase, is known from the equilibrium titrations, with the value used in these calculations, $\Delta F_{max} = 17$ (Figure 3). The solid lines in Figure 8 are nonlinear least-squares fits of eqs 21−24 to the experimental fractional individual amplitudes of the reaction. The fluorescence of the free MANT-ADP is taken as 1. The obtained data show that there is a large, similar increase of the MANT-ADP fluorescence upon forming the $(H-N)_1$, $(H-N)_2$, and $(H-N)_3$ with $\Delta F_2 = 16.6 \pm 1.5$, $\Delta F_3 = 14.2 \pm 1$, and $\Delta F_4 = 14.2 \pm 1$. These values are higher than the corresponding values obtained for MANT-AMP-PNP, indicating that the MANT moiety is closer to the tryptophans than in the complexes with ATP analogue. Also, contrary to MANT-AMP-PNP, the relative fluorescence intensity of the $(H-N)_4$ is strikingly higher ($\Delta F_5 = 35.5 \pm 5$). These results suggest that in the case of the ADP analogue the MANT group moves closer to the tryptophans in the $(H-N)_4$ than in the corresponding complex with MANT-AMP-PNP (see Discussion).

Binding of the Base-Modified Fluorescent Nucleotide Analogues, ϵAMP-PNP and ϵADP, to the Single, Noninteracting Site of the DnaB Helicase. Experiments with etheno-derivatives of AMP-PNP, ADP, ϵAMP-PNP, and ϵADP, with the fluorescent modification located on the base instead of on the ribose, provide an important and independent test of the determined mechanism of nucleotide binding and the role of the base in the recognition process. Binding of the etheno-derivative to the DnaB helicase is accompanied by a very modest nucleotide fluorescence intensity increase, which is not enough to quantitatively examine the complex kinetic mechanism of nucleotide binding (*21*, *28*). However, by adding an efficient collisional quencher to the solution, e.g., acrylamide, this low signal level can be amplified by more than an order of magnitude (*28*). We previously determined that acrylamide does not affect the free energy of binding of the etheno-derivatives to the DnaB helicase (*28*). Fluorescence titrations ($\lambda_{ex} = 325$ nm, $\lambda_{em} = 410$ nm) of ϵAMP-PNP and ϵADP, with the DnaB helicase in buffer T2 (pH 8.1, 100 mM NaCl, 20 °C) in the presence of 100 mM acrylamide, are shown in Figure 9. With the excitation wavelength at 325 nm, the fluorescence of the etheno-derivatives is predominantly observed. The maximum relative fluorescence increase of ϵAMP-PNP and ϵADP upon saturation with the DnaB helicase are $\Delta F_{max} = 2.7 \pm 0.3$ and $\Delta F_{max} = 3.4 \pm 0.3$, respectively. In the absence of acrylamide, analogous titrations produce only an ∼0.15 and ∼0.25 maximum increase of ϵAMP-PNP and ϵADP fluorescence upon saturation with the DnaB helicase (*28*).

The solid lines in Figure 9 are computer fits using a single site binding isotherm (eq 25). The obtained values of intrinsic binding constants K are $(6 \pm 1) \times 10^4$ M^{-1} and $(3.3 \pm 0.7) \times 10^5$ M^{-1} for ϵAMP-PNP and ϵADP, respectively (Table 1). Identical values have been obtained in the absence of acrylamide (data not shown). This result is expected because, as we determined before, acrylamide acts exclusively through the collisional quenching and does not have any detectable effect on the energetics of nucleotide binding (*28*). It is interesting that the fluorescence increase of ϵADP is significantly higher than that of ϵAMP-PNP (Figure 9). Thus, similar to the MANT derivatives, the equilibrium data already indicate that the conformational state of the ADP analogue in the helicase binding site is different from that of the ATP analogue, although in the case of the etheno-derivatives, the observed signal originates from the base (see Discussion).

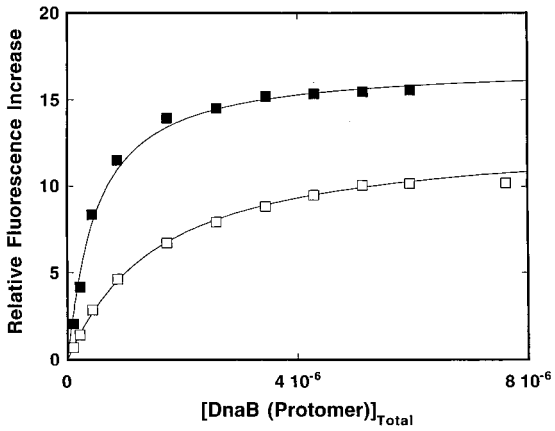

FIGURE 9: Fluorescence titrations of ϵAMP-PNP and ϵADP with the DnaB helicase in buffer T2 (pH 8.1, 100 mM NaCl, 20 °C) at different protein concentrations, ϵAMP-PNP (□), ϵADP (■). The solid lines are the best fits of the experimental isotherms to a single site isotherm (eq 25), using intrinsic binding constants $K = 6 \times 10^4$ (M^{-1}) and 3.3×10^5 (M^{-1}) for ϵAMP-PNP and ϵADP, respectively (see text for details). Concentrations of both nucleotides are 1.5×10^{-7} M.

Kinetics of the Base-Modified Fluorescent ATP Analogue, ϵAMP-PNP, Binding to a Single, Noninteracting Site on the DnaB Helicase. The stopped-flow kinetic trace of the ϵAMP-PNP fluorescence, after mixing the nucleotide (3×10^{-7} M) with the DnaB helicase [6×10^{-5} M (Protomer)], final concentrations, in buffer T2 (pH 8.1, 100 mM NaCl, 20 °C) containing 100 mM acrylamide, is shown in Figure 10. The trace has been recorded in two time bases, 0.5 and 200 s. As shown by the included deviations from the fit, the observed kinetic curve is adequately described by a four-exponential function, but not by a three-exponential function. Thus, similar to the MANT analogues, the association of ϵAMP-PNP with the single, noninteracting binding site of the DnaB helicase proceeds through at least four steps. However, there is a significant difference. While in the case of MANT analogues, the fluorescence increases monotonically with time, in the case of ϵAMP-PNP, the fluorescence intensity of the final equilibrium system is lower than the intensity at the intermediate time regions (Figure 10).

The reciprocal relaxation times, $1/\tau_1$, $1/\tau_2$, $1/\tau_3$, and $1/\tau_4$, characterizing the four binding processes, as a function of the total DnaB helicase concentration (Protomer), are shown in Figure 11. The functional dependence of the relaxation times is the same as observed for the MANT analogues (Figures 5 and 7). Thus, the largest reciprocal relaxation time, $1/\tau_1$, characterizing the bimolecular binding step, increases with the [DnaB], while $1/\tau_2$, $1/\tau_3$, and $1/\tau_4$ reach plateaus at high enzyme concentrations. Therefore, binding of the ϵAMP-PNP analogue to the single, noninteracting nucleotide-binding site of the DnaB helicase can be described by the same mechanism as determined for the MANT analogues in which the bimolecular association is followed by three conformational transitions of the formed complex (Scheme 1). In other words, the general mechanism of nucleotide

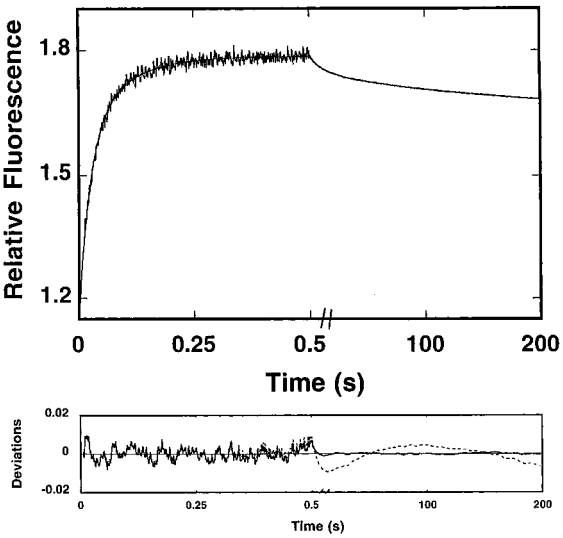

FIGURE 10: Top panel is the fluorescence stopped-flow kinetic trace, recorded in two time bases, 0.5 and 200 s, after mixing the DnaB with ϵAMP-PNP in buffer T2 (pH 8.1, 100 NaCl, 20 °C) (λ_{ex} = 325 nm, λ_{em} > 400 nm). The final concentrations of the helicase and the nucleotide are 6×10^{-5} M (Protomer) and 3×10^{-7} M, respectively. The solid line is the four-exponential, nonlinear least-squares fit of the experimental curve using eq 1. The lower panel shows the deviation of the experimental curve from the fit using a three-exponential (---) and a four-exponential (—) function, respectively (eq 1).

binding is independent of nucleotide modification, although the rate constants, determined using the nonlinear least-squares fit (solid lines in Figure 11), characterizing the reaction steps are significantly different (Table 2).

Molar fluorescence intensities characterizing each intermediate of the reaction, relative to the molar fluorescence of the free ϵAMP-PNP, have been obtained by analyzing the individual amplitudes of the reaction using the matrix projection operator technique described above (data not shown). The obtained data indicate that formation of the $(H-N)_1$ and $(H-N)_2$ is accompanied by the large fluorescence increase of ϵAMP-PNP with $\Delta F_2 = 5.3 \pm 1$ and $\Delta F_3 = 4.3 \pm 1$ (Table 2). However, the relative fluorescence of the $(H-N)_3$ is significantly lower with $\Delta F_4 = 1.8 \pm 0.6$. On the other hand, transition to the $(H-N)_4$ is accompanied by a significant fluorescence increase with $\Delta F_4 = 3.7 \pm 1$. These results suggest that the location of the base of the bound nucleotide is different in different intermediates, with the base being exposed the most to the solvent in the $(H-N)_3$ complex (see Discussion).

Kinetics of the Base-Modified Fluorescent ADP Analogue, ϵADP, Binding to the DnaB Helicase. Similar to all studied nucleotide analogues, the stopped-flow kinetic traces of the ϵADP fluorescence, after mixing the nucleotide with the helicase, require the four-exponential function to describe the experimental curves (data not shown). Also, as in the case of ϵAMP-PNP, but contrary to the MANT analogues, the fluorescence intensity of the final equilibrium system is lower than the intensity at the intermediate time regions.

The reciprocal relaxation times, $1/\tau_1$, $1/\tau_2$, $1/\tau_3$, and $1/\tau_4$, as a function of the total DnaB helicase concentration (Protomer) are shown in Figure 12. The solid lines in Figure 12 are computer fits of the relaxation times according to the four-step mechanism (Scheme 1) with the rate constants and equilibrium constants for the individual steps included in

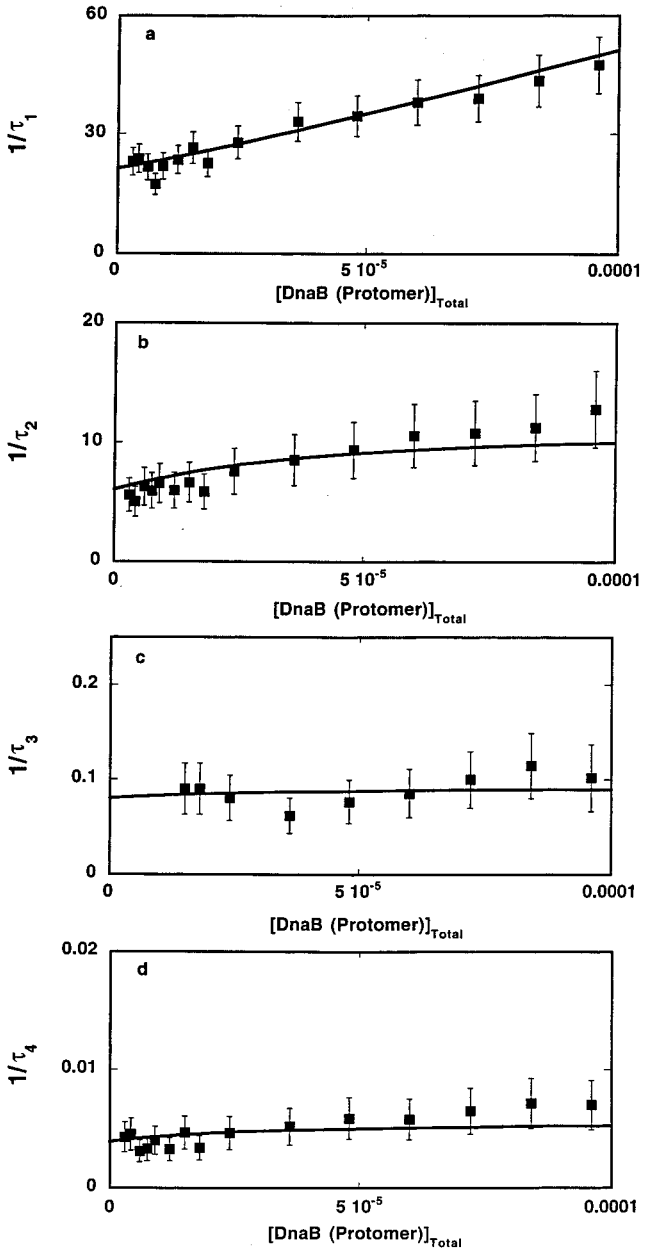

FIGURE 11: Dependence of the reciprocal of the relaxation times for the binding of ϵAMP-PNP to the DnaB helicase in buffer T2 (pH 8.1, 100 mM NaCl, 20 °C) upon the total concentration of the helicase (Protomer). The solid lines are nonlinear least-squares fits according to the four-step sequential mechanism, defined by Scheme 1, with the rate constants $k_1 = 3.4 \times 10^5$ M^{-1} s^{-1}, $k_{-1} = 16$ s^{-1}, $k_2 = 3.3$ s^{-1}, $k_{-2} = 8$ s^{-1}, $k_3 = 0.05$ s^{-1}, $k_{-3} = 0.07$ s^{-1}, $k_4 = 0.01$ s^{-1}, and $k_{-4} = 0.0045$ s^{-1}; (a) $1/\tau_1$, (b) $1/\tau_2$, (c) $1/\tau_3$, (d) $1/\tau_4$. The error bars are standard deviations obtained from three to four independent experiments.

Table 2. The major difference between ϵADP and ϵAMP-PNP is in the value of the association bimolecular rate constant, k_1, which for the ADP analogue is an order of magnitude higher than in the case of ϵAMP-PNP, while k_{-1} has similar values (Table 2). Notice, MANT-ADP also has the forward rate constant, k_1, for the bimolecular step, which is higher than the one determined for MANT-AMP-PNP (Table 2). As a result, the bimolecular binding step is energetically much more favorable for ADP analogues and is mainly responsible for the higher affinity of the ADP analogues for the nucleotide-binding site than the ATP analogues (*19*−*22*).

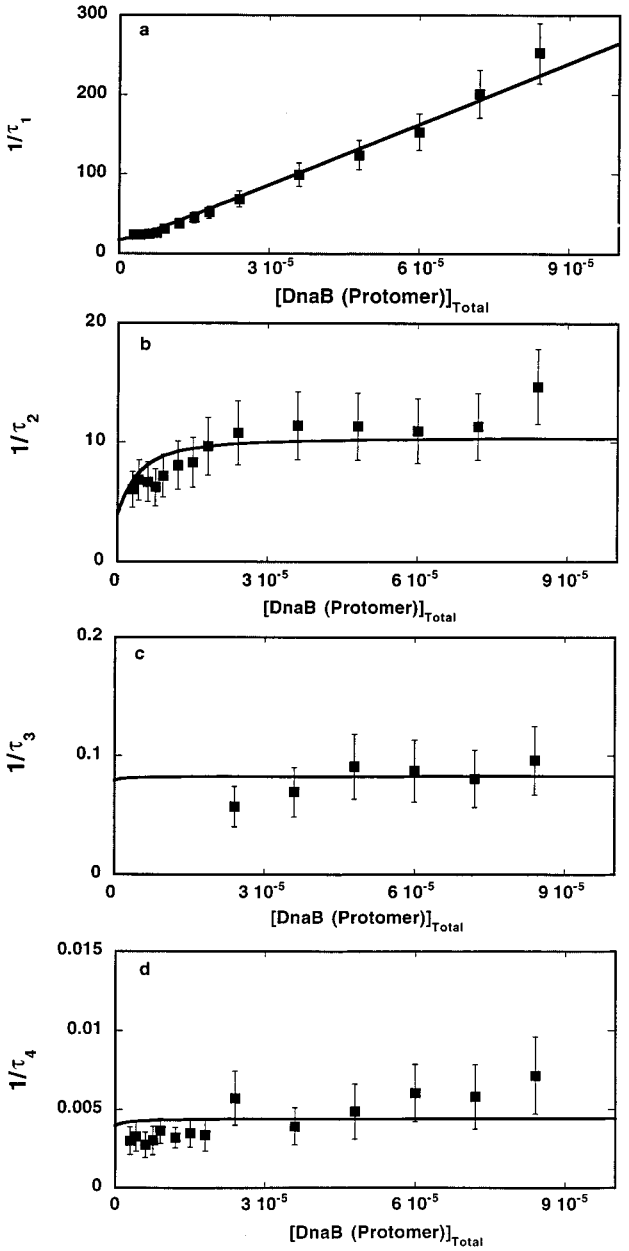

FIGURE 12: Dependence of the reciprocal of the relaxation times for the binding of ϵADP to the DnaB helicase in buffer T2 (pH 8.1, 100 mM NaCl, 20 °C) upon the total concentration of the helicase (Protomer). The solid lines are nonlinear least-squares fits according to the four-step sequential mechanism, defined by eq 2, with the rate constants $k_1 = 2.6 \times 10^6$ M^{-1} s^{-1}, $k_{-1} = 10$ s^{-1}, $k_2 = 4$ s^{-1}, $k_{-2} = 6.5$ s^{-1}, $k_3 = 0.01$ s^{-1}, $k_{-3} = 0.07$ s^{-1}, $k_4 = 0.009$ s^{-1}, and $k_{-4} = 0.0045$ s^{-1}; (a) $1/\tau_1$, (b) $1/\tau_2$, (c) $1/\tau_3$, (d) $1/\tau_4$. The error bars are standard deviations obtained from three to four independent experiments.

The dependence of the fractional individual amplitudes, A_1, A_2, A_3, and A_4, of all four relaxation steps upon the logarithm of the total DnaB concentration (Protomer), is shown in Figure 13. The solid lines in Figure 13 are nonlinear least-squares fits of eqs 21−24 to the experimental fractional individual amplitudes of the reaction with the fluorescence of the free ϵADP taken as 1. The obtained data indicate that formation of the $(H-N)_1$, $(H-N)_2$, and $(H-N)_3$ is accompanied by a large fluorescence increase of ϵADP, with $\Delta F_2 = 4.6 \pm 0.7$, $\Delta F_3 = 4.9 \pm 0.7$, and $\Delta F_4 = 2.5 \pm 0.6$. The data suggest that in all these intermediates the base is significantly shielded from the solvent. On the other hand,

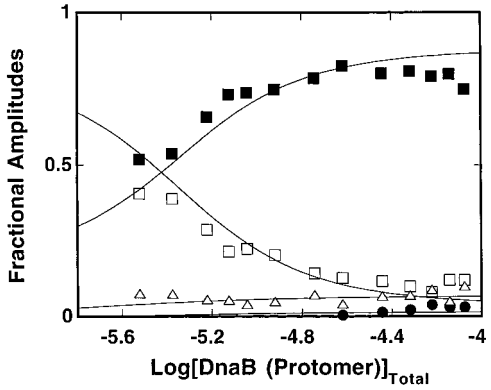

FIGURE 13: Dependence of the individual relaxation amplitudes of the kinetic process of ϵADP binding to the DnaB helicase in buffer T2 (pH 8.1, 100 mM NaCl, 20 °C) upon the logarithm of the total concentration of the enzyme (Protomer). The solid lines are computer fits according to the four-step sequential mechanism using eqs 21−24, with the relative fluorescence intensities $\Delta F_2 = 4.6$, $\Delta F_3 = 4.9$, $\Delta F_4 = 2.5$, and $\Delta F_5 = 1.1$. The fluorescence intensity of the free ϵADP is taken as $\Delta F_1 = 1$. The maximum fluorescence increase of the nucleotide has been determined in the equilibrium fluorescence titration as $\Delta F_{max} = 3.7$ (Figure 9). The rate constants are the same as obtained from the relaxation time analysis (Figure 13, Table 2); A_1 (■), A_2 (□), A_3 (●), A_4 (△).

contrary to ϵAMP-PNP, transition to the $(H-N)_4$ leads to the complex with $\Delta F_5 = 1.1 \pm 0.3$. This result suggests that in the last intermediate the base becomes completely exposed to the solvent (see Discussion).

DISCUSSION

Binding and/or hydrolysis of ribonucleotide triphosphates (rNTPs) are crucial in regulating the functions of the DnaB helicase (*1*, *3*, *5*, *18*). On the bases of thermodynamically rigorous fluorescence titrations, we previously determined that the DnaB protein has six nucleotide-binding sites and that negative cooperative interactions exist between the sites (*19*−*22*, *28*). Thermodynamically, a hexagon model describes the DnaB hexamer where the cooperative interactions are limited to the two adjacent subunits (*19*). In the hexagon model, the first three nucleotide molecules bind to the three noninteracting sites. In other words, the binding of the first three nucleotides is equivalent to the binding to three independent sites on the enzyme. Only subsequent binding of the next three nucleotides is affected by the negative cooperative interactions with the high-affinity sites already saturated with the cofactors.

In this report, we address the kinetics of nucleotide cofactor binding to a single, noninteracting site on the DnaB helicase, using fluorescent nucleotide analogues, which differ by the type and location of the modifying group. In the case of MANT-AMP-PNP and MANT-ADP, the fluorescent group, methylantraniloyl (MANT), attaches to the ribose 2′ and/or 3′ oxygens, whereas in ϵAMP-PNP and ϵADP the modification is located on the adenine. In the case of the DnaB helicase, there is an effcient fluorescence energy transfer from the protein tryptophans to the fluorescent nucleotide analogue bound in the binding site (*6*). As a result, the fluorescence increase of the MANT derivatives is very strongly amplified when the excitation wavelength is in the tryptophan absorption band. We utilized this fact in the studies described in this work and monitored the kinetics of the binding of MANT derivatives through their fluorescence

increase resulting predominantly from the energy transfer from the protein tryptophans. A similar approach has been used in kinetic studies of the binding of MANT-derivatives to the *E. coli* Rep helicase (*29*, *30*). In the case of etheno-derivatives, the nucleotide fluorescence change, upon saturation with the DnaB helicase, is not enough to achieve the necessary resolution, even with the excitation through the fluorescence energy transfer from the tryptophan residues. In this case, we utilized the fact that the fluorescence of the free etheno-derivatives of the nucleotides is strongly quenched by the neutral quencher, acrylamide, exclusively through collisional quenching without affecting, to any detectable extent, the energetics of the cofactor binding (*19*, *28*). The fluorescence of the bound nucleotide is quenched by acrylamide to a much lesser extent, leading to more than an order of magnitude amplification of the nucleotide fluorescence upon saturation with the helicase (*28*).

Application of the Matrix Projection Operator Technique to Study Stopped-Flow Kinetics. Complex relaxation kinetics are usually studied either by purely numerical methods or by using approximate formulas for relaxation times and amplitudes (*26*). Purely numerical methods are very powerful but provide limited insight into the physical aspects of the studied mechanism. On the other hand, approximate formulas can very often be applied only in stringent conditions, which are not always fulfilled by the system. The matrix projection operator technique offers an experimenter the possibility of limiting the numerical analysis to finding only the eigenvalues of the coefficient matrix, which are directly related to the relaxation times of the kinetic system. Once the eigenvalues are determined, the amplitudes of each resolved step of the reaction can be explicitly defined in terms of rate constants, relaxation times, and spectroscopic properties of all intermediates by expanding the solution matrix using matrix projection operators (eqs 21−24).

Multiple-Step Kinetic Mechanism of Nucleotide Cofactor Binding to the Single, Noninteracting Binding Site on the DnaB Helicase. The results obtained in this work indicate that the mechanism of MANT-AMP-PNP and MANT-ADP binding to the single, noninteracting site on the DnaB helicase is a minimum four-step, sequential process described by Scheme 1. Thus, the nucleotide-binding site complex undergoes at least three conformational transitions following the initial complex formation. The same mechanism is observed for ϵAMP-PNP and ϵADP, indicating that the mechanism is independent of the location of the modification of the nucleotide. It also indicates that possible acyl-migration of the MANT moiety between the 2′ and 3′ OH group of the ribose is not affecting the fundamental characteristic of the determined mechanism (*24*). In other words, the four-step sequential mechanism is an intrinsic property of the DnaB helicase−nucleotide system.

In most chemical bimolecular reactions, formation of the product is preceded by a collision−encounter complex, a process that is controlled by diffusion of the reactants (*31*, *32*). It should be noted that the highest value of the bimolecular association rate constant observed for MANT-ADP is $k_1 = (3.5 \pm 1) \times 10^6\ M^{-1}\ s^{-1}$, which is significantly lower than that expected for the diffusion-controlled reaction (*31*, *32*). The values of k_1 determined for the other nucleotides are even lower (Table 2). Theoretical values of the maximum rate constant for the diffusion-controlled association can be estimated using the Smoluchowski equation (32)

$$k_D = \frac{4\pi N_A (D_P + D_D)(r_P + r_D)}{1000} \tag{28}$$

where N_A is Avogadro's number, D_P and D_D are diffusion coefficients of the protein and nucleotide, respectively, and r_P and r_D are their interaction radii. The diffusion coefficient of the DnaB helicase hexamer, $D_P = (2.8 \pm 0.3) \times 10^{-7}$ cm^2/s, has been determined using the dynamic light-scattering technique (Bujalowski, unpublished data). The diffusion coefficient of the nucleotide analogues can be estimated in the following way. The fluorescence anisotropy, r, and the lifetime, τ, of the free MANT-ADP, determined in our solution conditions, are $r = 0.015 \pm 0.005$ and $\tau = 3.9$ ns (*20*). The rotational correlation time of the nucleotide, modeled as a sphere, is determined by the formula (*33*)

$$\phi = \frac{r\tau}{r_o - r} \tag{29}$$

where r_o is the fundamental anisotropy of MANT-ADP (*20*). Using the r and τ values given above, and $r_o = 0.4$, one obtains the rotational correlation time of MANT-ADP, $\phi \approx 1.52 \times 10^{-10}$ s [buffer T2 (pH 8.1, 100 mM NaCl, 20 °C)]. The hydrated volume of the molecule, V_h, is related to the rotational correlation time, ϕ, by (*33*)

$$V_h = \frac{\phi kT}{\eta} \tag{30}$$

where k is the Boltzman constant, T is the temperature (Kelvin), and η is the viscosity of the solution. Introducing the value of ϕ into eq 30 gives $V_h \approx 4.73 \times 10^{-22}$ cm^3, which provides the radius of MANT-AMP-PNP, $r_b \approx 4.8$ Å. The translational diffusion coefficient is defined by the Stokes−Einstein equation as

$$D_b = \frac{kT}{6\pi r_b \eta} \tag{30}$$

Introducing the value of $r_b = 4.8$ Å provides $D_b = 3.42 \times 10^{-6}$ cm^2/s.

The interacting radii have been taken as equal to the approximate size of the radius of the nucleotide, $r_D = r_P \approx 4.8$ Å. With these values, the diffusion-controlled association rate constant, defined by eq 28, is $k_D \approx 2.7 \times 10^9\ M^{-1}\ s^{-1}$. Smaller interaction radii and/or orientation factors could lower this value to $k_D \approx 10^7 - 10^8\ M^{-1}\ s^{-1}$, which is a value similar to that observed for some fast formations of nucleotide cofactor−protein complexes (*34*). These estimates are approximate in nature; nevertheless, the determined bimolecular rate constant k_1 is ∼2−4 orders of magnitude lower than k_D, predicted by diffusion-controlled collision, suggesting that the bimolecular association step contains an additional conformational transition of the helicase−nucleotide complex. Strong evidence for the presence of the additional transition, following the collision complex, comes from the amplitude analysis which indicates that a large increase of the nucleotide fluorescence (large conformational change of the enzyme−nucleotide complex) occurs in the formation of the $(H-N)_1$. The very definition of the collision complex excludes such dramatic conformational changes of the heli-

Scheme 2

$$\text{Helicase} + \text{N} \underset{k_{-D}}{\overset{k_D}{\Leftrightarrow}} \text{E} \underset{k'_{-1}}{\overset{k'_1}{\Leftrightarrow}} (\text{H}-\text{N})_1 \underset{k_{-2}}{\overset{k_2}{\Leftrightarrow}} (\text{H}-\text{N})_2 \underset{k_{-3}}{\overset{k_3}{\Leftrightarrow}} (\text{H}-\text{N})_3 \underset{k_{-4}}{\overset{k_4}{\Leftrightarrow}} (\text{H}-\text{N})_4$$

case−nucleotide complex as a result of a simple collision (*31*, *32*). Therefore, Scheme 1 should be enlarged by an extra step following the collision complex, E, as described by Scheme 2 where k_D and k_{-D} are rate constants for the formation and dissociation of the collision complex and k'_1 and k'_{-1} are the rate constants for the transition from the collision complex to the $(H-N)_1$. The equilibrium constant for the first step is then $K_D = k_D/k_{-D}$. Because the formation of E is a very fast process and equilibrates before any significant transition to the $(H-N)_1$ takes place, the determined, apparent bimolecular rate constant is $k_1 = K_D\, k'_1$. It should be pointed out that we do not observe an amplitude lost in the dead time of the instrument (∼1.4 ms), which indicates that the collision process is very fast and there is no fluorescence change (conformational transition) accompanying its formation.

The estimate of the range of values for k'_1 can be obtained as follows. Notice, the dependence of the reciprocal relaxation time for the bimolecular process, $1/\tau_1$, e.g., for the MANT-AMP-PNP, is a linear function of the helicase concentration at the highest concentrations examined [$\sim 2 \times 10^{-5}$ M (Protomer)]. This shows that K_D is much lower than 5×10^4 M^{-1} (*26*). Taking a conservative value, $K_D \approx 10^3$ M^{-1}, gives $k'_1 \approx 900$ s^{-1} for MANT-AMP-PNP. Assuming the same conservative values of K_D, the corresponding values for MANT-ADP, ϵAMP-PNP, and ϵADP are 3500, 340, and 2600 s^{-1}. Thus, the data strongly suggest that the collision complex E undergoes a transition to the $(H-N)_1$, with a forward rate constant of more than ∼2 orders of magnitude larger, particularly for the ADP analogues, than the dissociation constant k_{-1} and the forward rate constants for subsequent formation of the $(H-N)_2$, $(H-N)_3$, and $(H-N)_4$.

Major Conformational Transition of the DnaB Helicase−Nucleotide Cofactor Complex Occurs in the First Binding Step. The functional dependence of the individual amplitudes, A_1, A_2, A_3, and A_4, of the relaxation processes in the DnaB helicase association reaction with all studied nucleotides fully supports the sequential character of the binding mechanism. Moreover, with the exception of MANT-ADP, the amplitude analysis indicates that the largest fluorescence increase, as compared with the free nucleotide, accompanies the formation of the $(H-N)_1$ complex.

Fluorescence energy transfer and dynamic collision with a quencher in solution are very fast processes occurring in the range of subnanoseconds (*33*). Also, the conformational dynamics of the nucleotide molecules is fast and proceeds in the range of nanoseconds (*35*). The fact that the transition from the collision complex E to the $(H-N)_1$ is characterized by a rate constant in the range of $\sim 300-3000$ s^{-1} indicates that this is not exclusively the rate of simple colliding with the area of the binding site, but rather a true conformational transition of the enzyme−nucleotide complex. In other words, the observed dynamics of the formation of the $(H-N)_1$ is an intrinsic property of the DnaB helicase, in response to nucleotide cofactor binding, and not simply an adjustment of the bound cofactor to the structure of the enzyme-binding site.

Amplitude Analysis Indicates Changing Location of the Base and MANT Moiety of the Bound Nucleotides in Different Intermediates. In the experiments described in this work, we followed the kinetics of the MANT derivatives by monitoring the fluorescence increase resulting predominantly from the fluorescence energy transfer from the protein tryptophan residues clustered around the nucleotide-binding site (*21*). In the case of the ATP analogue, MANT-AMP-PNP, the largest fluorescence increase in the formation of the $(H-N)_1$ suggests that the MANT group of the bound nucleotide is closest to the tryptophan residues in this intermediate. Lower values of ΔF_2 and ΔF_3 suggest that in the formation of subsequent intermediates, the group is placed farther away from the tryptophans and once again approaches these residues in the $(H-N)_4$, however, to a lesser extent than in the $(H-N)_1$. Although some specific rearrangements of the protein tryptophans cannot be excluded, much higher values of the relative molar fluorescence of all intermediates observed for MANT-ADP suggest that the MANT group is always closer to the tryptophan residues in the case of the ADP analogue. The major difference between MANT-AMP-PNP and MANT-ADP is in the value of ΔF_5. The error in determining ΔF_5 is large; however, it is still strikingly higher than any other fluorescence parameter, suggesting that in this complex the MANT group is much closer to the protein tryptophans than in any other intermediate, particularly, as compared to MANT-AMP-PNP.

The kinetics of ϵAMP-PNP and ϵADP are followed by monitoring the fluorescence increase resulting predominantly from the shielding of the base region of the nucleotide from the efficient collisional quencher, acrylamide (*20*, *28*). The data indicate that in the case of ϵAMP-PNP the base region of the bound nucleotide is shielded from the solvent in the $(H-N)_1$, $(H-N)_2$, and $(H-N)_4$. In the $(H-N)_3$, the base becomes transiently exposed to the solvent, suggesting that in this intermediate it partially leaves the cavity of the binding site (*20*). The behavior of ϵADP is different. The base is much more efficiently shielded from the solvent, as compared to ϵAMP-PNP, in the $(H-N)_1$, $(H-N)_2$, and $(H-N)_3$. However, with the transition to subsequent intermediates, the base becomes more and more exposed. In the $(H-N)_4$, the fluorescence of the bound nucleotide reaches the values of the fluorescence of the free cofactor in solution (Table 2).

We previously established, using fluorescence spectroscopy, that there are large structural differences between base- and ribose-binding regions of the nucleotide-binding site of the DnaB helicase (*20*). The results described above provide the first indications of significant structural differences between ATP and ADP bound to the nucleotide-binding site of the enzyme, in both the base- and ribose-binding regions.

Difference between the Energetics of Binding of the ADP and ATP Analogues to the DnaB Helicase Results Predominantly from the Differences in the Energetics of the First Binding Step. An interesting feature of the DnaB helicase interactions with nucleotide cofactors is the fact that the ADP analogues have a higher free energy of binding than the ATP analogues. So far, this has been found for all studied

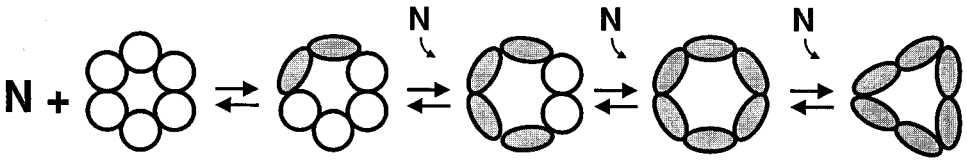

FIGURE 14: Schematic model of the sequential conformational transition of the entire DnaB hexamer, induced by nucleotide binding. Initially, all binding sites are independent, although quaternary interactions induce functional (possibly conformational) trimer of dimers structure of the six identical subunits. Binding of the first nucleotide molecule (N) to a single, independent binding site induces conformational changes of the two adjacent subunits (a dimer) of the hexamer. Binding of the second and third nucleotide molecules sequentially induced further structural changes of the next sets of two subunits. At this stage, with only the three bound nucleotide molecules, the major structural changes induced by nucleotide binding of the hexamer would be saturated (*6*). Further binding of the next, three nucleotide molecules does not induce additional global changes of the hexamer. This structure with C6 symmetry could be in equilibrium with the structure of C3 symmetry observed in E. M. studies (*9*).

nucleotide systems, ϵAMP-PNP/ϵADP, MANT-AMP-PNP/MANT-ADP, and TNP-ATP/TNP-ADP (*19*−*22*). The kinetic studies described in this work indicate that the major contribution to the free energy of binding is generated in the first binding step. The difference in the change of free energy in the first binding step between the ATP and ADP analogues results from the much higher apparent bimolecular association rate constant for the ADP analogues; this is particularly evident in the case of ϵAMP-PNP and ϵADP. The value of k_1 for ϵADP is approximately an order of magnitude higher than the value obtained for ϵAMP-PNP (Table 2).

Previously, we determined that binding of AMP-PNP induces a conformational change of the DnaB helicase which leads to an ~5 orders of magnitude increase of the affinity of the enzyme for the ssDNA (*7*). In the presence of ADP, the affinity for the ssDNA increases by only ~2 orders of magnitude. A plausible explanation of the observed lower free-energy change, in the case of ATP analogues, is that part of the free energy of binding of the nucleotide is used to induce the conformational transition of the DnaB leading to high ssDNA affinity (*36*). In the case of ADP, this transition is not complete and, as a result, requires much less of the free energy of nucleotide binding. The kinetic data described in this work strongly suggest that the conformational change, leading to a higher ssDNA affinity state, takes place in the first binding step, in the transition E $\leftrightarrow$ $(H-N)_1$. Notice, the difference is significantly lower in the free-energy change in the first binding step between the MANT-AMP-PNP/MANT-ADP system and ϵAMP-PNP/ϵADP (Table 2). This difference would result from the fact that both the γ phosphate and the ribose play a role in inducing a high ssDNA affinity state (*7*, *18*, *19*). In MANT-AMP-PNP, the ribose is partially blocked, thus, diminishing the ability to efficiently induce the conformational transition.

Comparison with Other Helicases. The kinetics of nucleotide analogue binding to the DnaB helicase is significantly different from the dynamics of the same nucleotide analogue binding to another well-studied *E. coli* Rep helicase (*29*, *30*). Kinetic data from Lohman's laboratory showed that the Rep helicase monomer binds nucleotide cofactors via a two-step mechanism, where fast bimolecular binding is followed by a single isomerization, although a third slow process has been observed for AMP-PNP in kinetic competition studies (*30*). The determined bimolecular rate constant for MANT-AMP-PNP ($\sim 7 \times 10^5$ M^{-1} s^{-1}) is very close to the value obtained for the DnaB helicase, although direct comparison is difficult due to different solution conditions. However, rate constants for the subsequent step (41 and 0.61 s^{-1}) are very different from the values of k_2 and k_{-2} determined for the DnaB helicase (Table 2).

The differences between the Rep and the DnaB helicases reflect very different structures and, most probably, different mechanisms of functioning. The Rep helicase exists in solution predominantly as a monomer which dimerizes upon complex formation with the DNA substrates (*17*). The DnaB helicase forms a ring-like structure in which protomer−protomer contacts are limited to two neighboring subunits (*6*, *8*, *9*). We obtained evidence, using the fluorescence energy transfer approach that, in the complex with the helicase, the ssDNA passes through the cross-channel of the hexamer (*16*). Similar structures of the equilibrium complexes between hexameric helicases and ssDNAs have been found in the case of bacteriophage T7 and T4 hexameric helicases (*37*−*39*). The functioning of the Rep helicase includes a complex dimerization of the enzyme at the ss- and dsDNA junction, with ATP and ADP controlling the enzyme interactions with the DNA substrates and differentially affecting the two subunits of the dimer (*40*−*42*). The DnaB helicase forms a stable hexamer in solution, specifically stabilized by multiple magnesium cation binding, and the binding of nucleotides induced global conformational transition of the entire hexamer (*6*, *9*). Moreover, we recently obtained evidence that the hexamer does not dissociate before binding to the ssDNA. The data indicate that the entry of the ssDNA into the cross-channel is accomplished by a local opening of the ring-like structure of the enzyme [Bujalowski and Jezewska, *J. Mol. Biol.* (in press)].

Sequential Character of the Mechanism of Nucleotide Binding to a Single, Noninteracting Nucleotide-Binding Site of the DnaB Helicase Excludes Preequilibrium Conformational Transition of the Enzyme. Experiments described in this work focus on the dynamics of nucleotide binding to a single, noninteracting site of the DnaB helicase. It should be pointed out that electron microscopy studies indicate that the DnaB hexamer exists in different conformations in the presence of nucleotide cofactors (*9*). Conformational changes of the hexamer induced by AMP-PNP and ADP have been observed in solution using the sedimentation velocity technique (*6*). The sequential mechanism of cofactor binding indicates that transitions to different states of the protein occur as a response to the formation of the enzyme−nucleotide complex. In other words, conformational transitions of the DnaB helicase, both the protomers and the entire hexamer, are not present prior to nucleotide binding but are induced by cofactor binding (*26*, *43*, *44*).

In the hexagon model of the binding of six nucleotide molecules to the DnaB helicase, the first three cofactors bind

to three independent sites on the hexamer (*19*−*22*). Only after these sites are saturated do the next nucleotide molecules bind with negative cooperativity. The excellent agreement between the overall intrinsic binding constant, determined in equilibrium fluorescence titrations and kinetic studies of a single site on the hexamer, with the intrinsic binding constant, determined from the analysis of the entire binding isotherm, using the hexagon model, provides very strong evidence that all six nucleotide-binding sites are initially independent.

As we pointed out, the negative cooperative interactions are limited to the two adjacent subunits and are induced by the binding of the first nucleotides (*19*−*22*). Thus, equilibrium and kinetic data suggest that the sequential conformational changes resulting from the binding of a nucleotide to the single, noninteracting site include at least one of the subunits adjacent the subunit bound with the nucleotide. On the other hand, E. M. data strongly suggest that the DnaB hexamer is assembled as a trimer of dimers (*8*, *9*, *45*). Recall, the binding of both AMP-PNP and ADP induces a global change in the structure of the entire DnaB hexamer, as seen by hydrodynamic and E. M. techniques (*6*, *9*). In fact, these large changes become gradually saturated with only three out of six binding sites of the hexamer being saturated with the nucleotides (*6*). Because, the binding sites are initially independent, these data suggest that conformational changes of the hexamer are sequential and induced by the initial binding of the nucleotide molecules to the independent sites. A model of the sequential conformational transition of the entire DnaB hexamer, which can account for all these data, is depicted in Figure 14. Binding of the first nucleotide molecule to an independent binding site induces conformational changes of the two adjacent subunits (a dimer) of the hexamer. Binding of the second and third nucleotides sequentially induced further structural changes of the next sets of the two subunits. Thus, saturation of the hexamer with the first three nucleotide molecules would induce most of the global conformational changes observed by hydrodynamic methods (*6*).

ACKNOWLEDGMENT

We wish to thank Gloria Drennan Davis for her help in preparing the manuscript.

REFERENCES

1. Kornberg, A., and Baker, T. A. (1992) *DNA Replication*, Freeman, San Francisco.
2. Matson, S. W., and Kaiser-Rogers, K. A. (1990) *Annu. Rev. Biochem. 59*, 289−329.
3. LeBowitz, J. H., and McMacken, R. (1986) *J. Biol. Chem. 261*, 4738−4748.
4. Baker, T. A., Funnell, B. E., and Kornberg, A. (1987) *J. Biol. Chem. 262*, 6877−6885.
5. Reha-Krantz, L. J., and Hurwitz, J. (1978) *J. Biol. Chem. 253*, 4051−4057.
6. Bujalowski, W., Klonowska, M. M., and Jezewska, M. J. (1994) *J. Biol. Chem. 269*, 31350−31358.
7. Jezewska, M. J., and Bujalowski, W. (1996) *J. Biol. Chem. 271*, 4261−4265.
8. San Martin, M. C., Stamford, N. P. J., Dammerova, N., Dixon, N. E., and Carazo, J. M. (1995) *J. Struct. Biol. 114*, 167−176.
9. Yu, X., Jezewska, M. J., Bujalowski W., and Egelman. E. H. (1996) *J. Mol. Biol. 259*, 7−14.
10. Jezewska, M. J., Kim, U.-S., and Bujalowski, W. (1996) *Biochemistry 36*, 2129−2145.
11. Jezewska, M. J., and Bujalowski, W. (1996a) *Biochemistry 35*, 2117−2128.
12. Bujalowski, W., and Jezewska, M. J. (1995) *Biochemistry 34*, 8513−8519.
13. Jezewska, M. J., Rajendran, S., and Bujalowski, W. (1997) *Biochemistry 36*, 10320−10326.
14. Jezewska, M. J., Rajendran, S., and Bujalowski, W. (1998) *Biochemistry 37*, 3116−3136.
15. Jezewska, M. J., Rajendran S., and Bujalowski. W. (1998) *J. Biol. Chem. 273*, 9058−9069.
16. Jezewska, M. J., Rajendran S., Bujalowska, D., and Bujalowski, W. (1998) *J. Biol. Chem. 273*, 10515−10529.
17. Lohman, T. M., and Bjorson, K. P. (1996) *Annu. Rev. Biochem. 65*, 169−214.
18. Arai, K., and Kornberg, A. (1981) *J. Biol. Chem. 256*, 5260−5266.
19. Bujalowski, W., and Klonowska, M. M. (1993) *Biochemistry 32*, 5888−5900.
20. Bujalowski, W., and Klonowska, M. M. (1994) *Biochemistry 33*, 4682−4694.
21. Bujalowski, W., and Klonowska, M. M. (1994) *J. Biol. Chem. 269*, 31359−31371.
22. Jezewska, M. J., Kim U.-S., and Bujalowski W. (1996) *Biophys. J. 71*, 2075−2086.
23. Secrist, J. A., Bario, J. R., Leonard, N. J., and Weber, G. (1972) *Biochemistry 11*, 3499−3506.
24. Hiratsuka, T. (1983) *Biochim. Biophys. Acta 742*, 496−508.
25. Pilar, F. L. (1968) *Elementary Quantum Cemistry*, Chapter 9, McGraw-Hill, New York.
26. Bernasconi, C. F. (1976) *Relaxation Kinetics*, Academic Press, New York.
27. Fraser, R. A., Duncan, W. J., and Collar, A. R. (1965) *Elementary Matrixes and Some Applications to Dynamics and Differential Equations*, Cambridge University Press.
28. Jezewska, M. J., and Bujalowski, W. (1997) *Biophys. Chem. 64*, 253−269.
29. Moore, J. K., and Lohman, T. M. (1994) *Biochemistry 33*, 14550−14564.
30. Moore, J. K., and Lohman, T. M. (1994) *Biochemistry 33*, 14565−14578.
31. Berry, R. S., Rice, S. A., and Ross, J. (1980) *Physical Chemistry*, J. Wiley & Sons, New York.
32. Moore, J. W., and Pearson. R. G. (1981) *Kinetics and Mechanism*, J. Wiley & Sons, New York.
33. Lakowicz, J. R. (1999) *Principle of Fluorescence Spectroscopy*, Kluwer Academic/Plenum Publishers.
34. Hammes, G. G., and Schimmel, P. R. (1970) *The Enzymes. Kinetics and Mechanism*, Vol. II, Chapter 2, Academinc Press, New York.
35. Baker, B. M., Vanderkooi, J., and Kallenbach, N. R. (1978) Base Stacking in a Fluorescent Dinucleotiside Monophosphate: ϵApϵA. *Biopolymers 17*, 1361−1372.
36. Jencks, W. P. (1980) *Adv. Enzymol. 51*, 75−106.
37. Dong, F., Gogol, E. P., and von Hippel, P. H. (1995) *J. Biol. Chem. 270*, 7462−7473.
38. Egelman, E. H., Yu, X., Wild, R., Hingorani, M. M., and Patel, S. S. (1995) *Proc. Natl. Acad. Sci. U.S.A. 92*, 3869−3873.
39. Hacker, K. J., and Johnson, K. A. (1997) *Biochemistry 36*, 14080−14087.
40. Bjorson, K. P., Moore, K. J., and Lohman, T. M. (1996) *Biochemistry 35*, 2268−2282.
41. Bjorson, K. P., Hsieh, J., Amaratunga, M., and Lohman, T. M. (1998) *Biochemistry 37*, 891−899.
42. Wong, I., Moore, K. J., Bjorson, K. J., Hsieh, J., and Lohman, T. M. (1996) *Biochemistry 35*, 5726−5734.
43. Bujalowski, W., Greaser, E., McLaughlin, L. W., and Porschke, D. (1986) *Biochemistry 25*, 6365−6378.
44. Bujalowski, W., Jung, M., McLaughlin, L. W., and Porschke, D. (1986) *Biochemistry 25*, 6372−6371.
45. San Martin, C., Radermacher, M., Wolpensinger, B., Engel, A., Miles, C. S., Dixon, N. E., and Carazo, J. M. (1998) *Structure 6*, 501−509.

BI992413M